Supplementary Information

Rhenium(I) and technetium(I) complexes with megazol derivatives: towards the development of a theranostic platform for Chagas disease

Ana C.R. Gonçalves,[1] Silvia H. Libardi,[2] Júlio C. Borges,[2] Ronaldo J. Oliveira,[1] Carla Gotzmann,[3] Olivier Blacque,[3] Sergio de Albuquerque,[4] Carla D. Lopes,[4,5*] Roger Alberto,[3] and Pedro I. S. Maia[1*]

[a.] *Bioactive Compounds Development Research Group, Federal University of Triângulo Mineiro, Av. Dr. Ran-dolfo Borges 1400, Uberaba 38025-440, MG, Brazil;*
[b.] *São Carlos Institute of Chemistry, University of São Paulo, Av. Trabalhador São Carlense, 400, São Carlos 13566-590, SP, Brazil;*
[c.] *Address here. Department of Chemistry, University of Zurich, Winterthurerstrasse 190, 8057 Zurich, Switzerland;*
[d.] *Department of Clinical, Toxicological and Bromatological Analysis, Faculty of Pharmaceutical Sciences of Ribeirão Preto - FCFRP-USP, University of São Paulo, Av. do Café s/n, 14040-903, Ribeirão Preto, SP, Brazil;*
[e.] *Ribeirão Preto's Estácio University Center, Abraão Issa Halach Street, 980, 14096-160, Ribeirão Preto, SP, Bra-zil;*

Table of Contents

Preparation of 1-methyl-5-nitro-1H-imidazole-2-carbaldehyde (NI2CA). Procedure 1: In a 100 mL reaction flask at N_2 environment, 0.500 g (3.18 mmol) of 1-methyl-5-nitro-1H-imidazole-2-methanol and 1.384 g (15.9 mmol) of activated manganese oxide were added in 20 mL of anhydrous toluene. The reaction was kept under reflux at 110 °C for 4 hours and then the supernatant isolated by centrifugation. The solution was dried, and the raw product purified by preparative HPLC. Reaction yield: 50.0 %.

Procedure 2: A 50 mL reaction flask containing 50 mg (0.318 mmol) of 1-methyl-5-nitro-1H-imidazole-2-methanol in 10 mL of DCM in an ice bath under continuously stirred for 10 minutes and was mixed with 1.5 equivalents of Dess-Martin Periodinan (202.3 mg, 0.477 mmol) and stirred 0 °C for 20 h. The resulting solution was filtered and extracted 3 times with 10 mL of saturated $Na_2S_2O_3$ solution, 3 times with 10 ml of saturated solution of $NaHCO_3$ and 1 time with saturated solution of NaCl. The organic phase was dried with magnesium sulfate and after evaporation an oily compound was obtained. The reaction yield was 50.0 %. UPLC retention time: 1.55 minutes ^{1}H NMR ($CDCl_3$-d_1, 500 MHz), δ/ppm: 9.95 (C-H(c), s, 1H), 8.12 (C–H(a), s). ^{13}C NMR ($CDCl_3$-d_1, 125.8 MHz), δ/ppm: 183.6 (C5), 143.1 (C4), 132.6 (C2) and 34.5 (C3), (C1 not found).

Preparation of (E)-2-(1-methyl-5-nitro-1H-imidazole-2-il)methyllene)hydrazine-1-carbotioamide derivatives – Tsc^{R,R}: Equimolar amounts of 1-methyl-5-nitro-1H-imidazole-2-carbaldehyde (220.8 mg; 1.42 mmol) and the desired thiosemicarbazide were dissolved in 5 mL of EtOH. After adding 3 drops of concentrated HCl to the solution, the reaction mixture was stirred at 80 °C under microwave radiation for 40 minutes. The reaction was followed by UPLC. After cooling to room temperature, the yellow precipitate formed was filtered, washed with EtOH (2 mL) and diethyl ether (5 mL), and dried under vacuum.

Tsc^{H,H} (R_1 = H; R_2 = H) - Reaction time: 40 minutes. UPLC retention time: 1.75 minutes Yield: 76.0% (246 mg). ^{1}H NMR (DMSO-d_6, 400 MHz), δ/ppm: 11.8 (s, 1H, NH), 8.6 (s, 1H, NH_2), 8.2 (s, 1H, N=CH), 8.1 (s, 1H, $CH_{imidazole}$), 7.8 (s, 1H, NH_2), 4.2 (s, 3H, CH_3). HR-ESI$^+$-MS (m/z, assignment): 229.05035, $[M+H]^+$ (calcd. 229.05022).

Tsc^{H,Me} (R_1 = H; R_2 = Me) – Reaction time: 40 minutes. UPLC retention time: 1.83 minutes. Yield: 47.3 % (163 mg). ^{1}H NMR (DMSO-d_6, 400 MHz), δ/ppm: 11.87 (s, 1H, NH), 8.31 (d, J = 4 Hz, 1H, NH), 8.19 (s, 1H, N=CH), 8.12 (s, 1H, $CH_{imidazole}$), 4.15 (s, 3H, CH_3), 3.03 (d, J = 4 Hz, 3H, $NHCH_3$). HR-ESI$^+$-MS (m/z, assignment): 243.06589, $[M+H]^+$ (calcd. 243.06587).

Tsc$^{Me, Me}$ (R_1 = Me; R_2 = Me) – Reaction time: 40 minutes. Yield: 55.4 % (201 mg). ^{1}H NMR (DMSO-d_6, 400 MHz), δ/ppm: 11.35 (s, 1H, NH), 8.32 (s, 1H, N=CH), 8.18 (s, 1H, $CH_{imidazole}$), 4.30 (s, 3H, CH_3), 3.31 (s, 6H, $N(CH_3)_2$). HR-ESI$^+$-MS (m/z, assignment): 257.08129, $[M+H]^+$ (calcd. 257.08152).

HPLC and UPLC. The UPLC-ESI-MS measurements were performed using a UPLC Waters Acquity coupled to a Bruker HCT™, with a column Acquity UPLC BEH C18 1.7 μm (2.1 x 50 mm) and wavelength 200 – 800 nm, considering the m/z values for the most intense signal. UPLC-MS analyses were carried out using the linear gradient method of A (acetonitrile (Sigma-Aldrich HPLC grade)) and B (distilled water containing 0.1 % formic acid): t = 0-0.5 min, 5 % A; t = 4.0 min, 100 % A, t = 5.0 min, 100 % A. The flow speed is 0.6 mL/min. Analytical UPLC data were acquired using a VWR Hitachi Chrommaster Ultra, using Column Acquity UPLC BEH C18 1.7 μm (2.1 x 50 mm) using a linear gradient of A (acetonitrile (Sigma-Aldrich HPLC-grade)) and B (distilled water containing 0.1% TFA): t = 0-0.5 min, 5% A; t = 4.0 min, 100% A, t = 5.0 min, 100 % A. The flow speed is 0.5 mL/min. Preparative HPLC system was a Varian ProStar 320 with a Dr. Maisch Reprosil C18 100-7 (40 x 250 mm) column with a linear gradient of A (acetonitrile (Sigma-Aldrich HPLC-grade)) and B (distilled water with 0.1% TFA): t = 0 - 50 min, 30 - 100% A, flow rate 40 mL/min. RadioHPLC analysis were performed using a Merck Hitachi LaChrome system with a Merck Hitachi D-7000 autosampler interface, coupled to a Merck Hitachi LaChrome L-7400 UV detector equipped with a photodiode array. The radioactive detection of ^{99m}Tc complexes was obtained using a Berthold Technologies Flowstar LB513 detector equipped with BGO-X (γ) cells. The radioHPLC analyses were acquired using a gradient method of solvent A (MeOH, Sigma-Aldrich HPLC-grade) and solvent B (distilled water containing 0.1% formic acid): t = 0 – 3 min, 10% A; t = 3 – 3.1 min, 10 – 25% A; t = 3.1 – 9 min, 25% A; t = 9 – 9.1 min, 25 - 34% A; t = 9.1 – 20 min, 34 – 100% A; t = 20 – 25 min, 100% A; t = 25 – 25.1 min, 100% A; t = 25.1 – 30 min 100% A. Flow rate was 0.5 mL/min.

TABLES

Table S1 – Refinement data for $Tsc^{H,Me}$, $Tsc^{Me,Me}$, $L^{H,H}$, $L^{H,Me}$, $[ReBr(CO)_3(L^{H,H})]\cdot C_3H_6O$ (**1**$\cdot C_3H_6O$) and $[ReBr(CO)_3(L^{Me,Me})]$ (**3**).

	$Tsc^{H,Me}$	$Tsc^{Me,Me}$	$L^{H,H}$	$L^{H,Me}$	**1**$\cdot C_3H_6O$	**3**
Formula	$C_7H_{10}N_6O_2S$	$C_8H_{12}N_6O_2S$	$C_6H_6N_6O_2S$	$C_7H_8N_6O_2S$	$C_{12}H_{12}BrN_6O_6ReS$	$C_{11}H_{10}BrN_6O_5ReS$
MM	242.27	256.30	226.23	240.25	634.45	604.42
Crystal System	Monoclinic	Monoclinic	Monoclinic	Monoclinic	Orthorhombic	Orthorhombic
Space Group	$P2_1/c$	$P2_1/c$	$P2_1/c$	$P2_1/n$	$Pca2_1$	$Pbca$
a (Å)	7.83761(15)	6.7222(3)	11.6955(10)	5.67495(16)	14.84927(20)	12.8669(5)
b (Å)	10.32677(19)	28.6428(14)	5.6150(5)	9.4303(2)	11.36267(14)	8.9140(3)
c (Å)	13.6972(2)	6.0461(3)	14.3386(14)	18.9778(5)	11.34831(14)	29.5706(12)
α (°)	90	90	90	90	90	90
β (°)	99.9473(17)	106.054(5)	95.919(9)	95.371(3)	90	90
γ (°)	90	90	90	90	90	90
V (Å^3)	1091.95(4)	1118.73(10)	936.60(15)	1011.17(5)	1914.77(4)	3391.6(2)
Z	4	4	4	4	4	8
ρ_{calcd} (g·cm^{-3})	1.474	1.522	1.604	1.578	2.201	2.367
μ (mm^{-1})	2.656	0.291	3.058	2.868	16.277	9.681
Reflections Collected	8233	20845	6459	9328	17726	26767
Independent	2225/0.0165	2288/0.0335	1882/0.0820	2026/0.0344	3301/0.0326	5186/0.0538

reflections/R_{int}						
Data/restrictions/param.	2225/0/155	2288/0/161	1882/0/145	2026/0/151	3301/13/255	5186/3/239
Absorption Correction	Analytical	Analytical	Analytical	Analytical	Analytical	Analytical
Max/min. Transmission	0.763/0.615	0.981/0.920	0.957/0.788	0.911/0.669	0.771/0.274	0.540/0.286
R_1 [$I > 2\sigma(I)$]	0.0289	0.0299	0.0475	0.0415	0.0211	0.0387
wR_2 [$I > 2\sigma(I)$]	0.0780	0.0749	0.1097	0.1146	0.0555	0.0641
GOF	1.059	1.061	1.016	1.075	1.083	1.230
CCDC N°	2366616	2366617	2366618	2366619	2366620	2366621

Table S2– ^{1}H NMR data of the organic compounds: chemical shifts (δ, ppm), multiplicity (M) and integrals (I).

	N12CA- $CDCl_3$-*d* 500 MHz			$tsc^{H,H}$ DMSO-d_6 400 MHz			$L^{H,H}$ DMSO-d_6 500 MHz		
	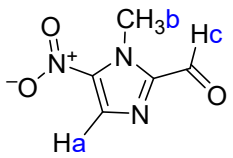			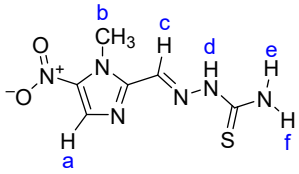			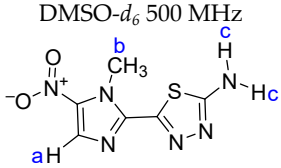		
	δ	M	I	δ	M	I	δ	M	I
a	8.1	s	1H	8.1	s	1H	8.5	s	1H
b	4.4	s	3H	4.2	s	3H	4.9	s	3H
c	9.9	s	1H	8.2	s	1H	-	-	2H
d	-	-	-	11.8	s	1H	-	-	-
e,f	-	-	-	8.6 and 7.8	s	2H	7.6	s	-
	N12CA $CDCl_3$-*d* 500 MHz			$tsc^{H,Me}$ DMSO-d_6 400 MHz			$L^{H,Me}$ DMSO-d_6 500 MHz		
	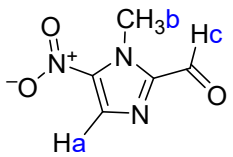			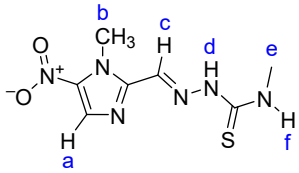			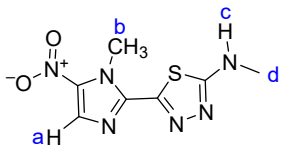		
	δ	M	I	δ	M	I	δ	M	I
a	8.1	s	1H	8.1	s	1H	8.2	s	1H
b	4.4	s	3H	4.1	s	3H	4.3	s	3H
c	9.9	s	1H	8.2	s	1H	8.3	d	1H
d	-	-	-	11.9	s	1H	3.0	d	3H
e	-	-	-	3.0	d	3H	-	-	-
f	-	-	-	8.3	d	1H	-	-	-
	N12CA $CDCl_3$-*d* 500 MHz			$tsc^{Me,Me}$ DMSO-d_6 400 MHz			$L^{Me,Me}$ DMSO-d_6 500 MHz		
	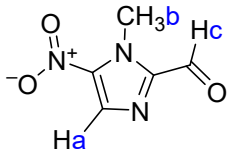			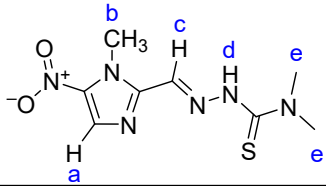			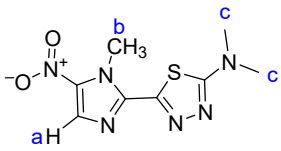		
	δ	M	I	δ	M	I	δ	M	I
a	8.1	s	1	8.2	s	1H	8.2	s	1H
b	4.4	s	3	4.3	s	3H	4.3	s	3H
c	9.9	s	1	8.3	s	1H	3.2	-	6H
d	-	-	-	11.3	s	1H	-	-	-
e	-	-	-	3.3	s	6H	-	-	-

Table S3 – Predicted and experimental signals by DEPT experiments for megazol compared to the aldehyde precursor.

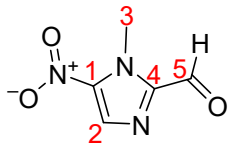

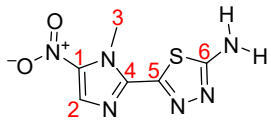

	δ/ppm	Predicted	DEPT 135	DEPT 90	δ/ppm	Predicted	DEPT 135	DEPT 90
1	-	143.2	-	-	141.5	138.7	-	-
2	132.6	132.0	+	+	133.2	132.3	+	+
3	34.5	35.8	+	–	35.1	26.6	+	–
4	143.1	141.3	-	-	140.2	155.0	-	-
5	183.6	183.6	+	+	170.0	161.6	-	-
6	-	-	-	-	148.3	174.1	-	-

Table S4 – Selected IR bands for the free ligands $\mathbf{L^{R1,R2}}$ and their complexes $[ReBrL^{H,H}(CO)_3]\cdot C_3H_6O$ (**1**), $[ReBr(CO)_3L^{Me,H}]$ (**2**) and $[ReBr(CO)_3L^{Me,Me}]$ (**3**).

	υ(N–H)	υ(C≡O)	δ(C–N)+ν(C–NH$_2$)	υ(C=N)+(C=C)	υ(N–O)$_{as}$	υ(N–O)$_{s}$	υ(C–S)
$\mathbf{L^{H,H}}$	3428*w* 3280*w*	-	1632*m*	1518*m*	1494*s*	1365*s*	1336*s*
1	3407*m* 3236*m*	2032*s* 1929*s* 1896*s*	1597*s*	1528*s*	1497*s*	1384*s*	1282*s*
$\mathbf{L^{H,Me}}$	3193*w*	-	1583*m*	1536*s*	1523*s*	1362*s*	1332*s*
2	3216*m*	2033*s* 1931*s* 1911*s*	1556*s*	1529*s*	1503*s*	1372*s*	1280*s*
$\mathbf{L^{Me,Me}}$	-	-	1555s	1532s	1513*s*	1397*s*	1362*s*
3	-	2024*s* 1922*s* 1886*s*	1577s	1530s	1531*s*	1374*s*	1309*m*

Table S5 – Selected Bond lengths (Å) and bond angles (°) for the organic compounds.

	$\mathbf{tsc^{H,Me}}$	$\mathbf{tsc^{Me,Me}}$	$\mathbf{L^{H,H}}$	$\mathbf{L^{H,Me}}$
Bond Lengths				
N1−O1	1.2213(15)	1.2306(17)	1.222(4)	1.232(3)
N1−O2	1.2249(16)	1.2309(16)	1.229(4)	1.233(3)
N1−C1	1.4192(15)	1.4216(18)	1.429(4)	1.419(3)
N3−C2	1.3506(15)	1.3542(18)	1.356(4)	1.353(3)
N3−C4	1.3422(16)	1.3429(18)	1.335(4)	1.341(3)
N4−C5	1.2886(16)	1.2916(19)	1.304(4)	1.302(3)
N4−N5	1.3587(15)	1.3566(17)	1.383(4)	1.367(2)
S1−C6	1.6812(14)	1.6837(14)	1.734(3)	1.740(2)
N6−C6	1.3200(17)	1.3369(19)	1.341(4)	1.334(3)
Bond Angles				
O1−N1−O2	123.21(11)	123.99(13)	124.3(3)	123.59(19)
C2−N3−C4	105.82(10)	105.99(12)	105.7(3)	105.31(17)
C5−N4−N5	118.60(11)	117.54(12)	112.7(3)	113.13(17)
S1−C6−N6	126.41(10	124.34(11)	121.6(2)	122.60(16)

Table S6 – ^{1}H NMR data of the complexes **1**, **2** and **3**: chemical shifts (δ, ppm), multiplicity (M) and integrals (I).

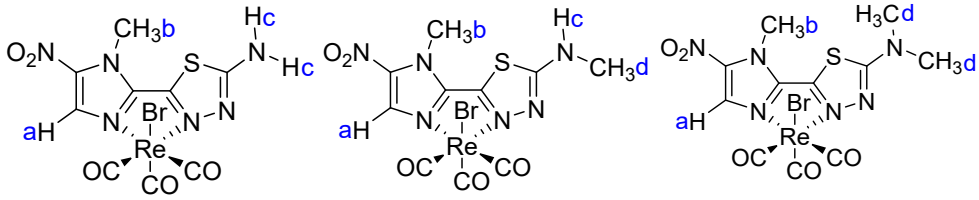

	δ	M	I	δ	M	I	δ	M	I
a	8.7	s	1H	8.6	s	1H	8.6	s	1H
b	4.5	s	3H	4.4	s	3H	4.5	s	3H
c	7.98	s	1H	8.2	s	1H	-	-	-
d	-	-	-	3.2	s	1H	3.4	-	6H

Table S7 - Predicted and experimental signals by ^{13}C NMR and DEPT experiments of the complexes in acetone-d_6.

L^{H,H} Acetone $-d_6$

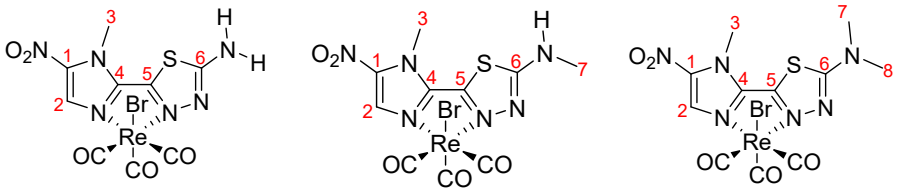

	δ/ppm	δ/ppm	DEPT 135	DEPT 90	δ/ppm	DEPT 135	DEPT 90	δ/ppm	DEPT 135	DEPT 90
1	142.8	147.7	-	-	146.3	-	-	146.0	-	-
2	133.4	133.9	+	+	133.9	+	+	133.8	+	+
3	35.7	36.4	+	–	36.2	+	–	36.2	+	–
4	141.5	141.0	-	-	140.9	-	-	140.9	-	-
5	170.8	172.1	+	+	147.9	+	+	173.8	+	+
6	150.7	147.9	-	-	172.9	-	-	147.9	-	-
7	-	-	-	-	32.8	+	–	41.9	+	–
8	-	-	-	-		-	-	41.9	+	–
CO	-	197.3	-	-	188.4	-	-	188.4	-	-
CO	-	188.5	-	-	197.1	-	-	197.1 /197.2	-	-

Table S8. Selected bond lengths (Å) and angles (°) for the complexes **1** and **3**.

	1	**3**		**1**	**3**
Bond lengths					
N1−O1	1.221(9)	1.212(6)	C11−O11	1.140(9)	1.145(6)
N1−O2	1.234(9)	1.212(6)	C12−O12	1.133(8)	1.148(6)
N3−C2	1.303(8)	1.357(6)	C13−O13	1.097(9)	1.125(10)/1.126(11)
N3−C4	1.371(8)	1.344(6)	N3−Re1	2.177(5)	2.180(4)
C4−C5	1.447(8)	1.436(7)	N4−Re1	2.168(5)	2.174(4)
N4−N5	1.369(8)	1.351(5)	Br1−Re1	2.6274(8)	2.6055(7)/2.549(4)
C5−N4	1.303(8)	1.326(6)	Re1−C13	1.936(7)	1.969(7)/1.969(9)
C5−S1	1.726(6)	1.724(5)	Re1−C11	1.927(7)	1.914(6)
C6−S1	1.773(7)	1.763(5)	Re1−C12	1.930(6)	1.917(5)
Bond angles					
Re1−N3−C4	115.9(4)	115.3(3)	N4−Re1−Br1	83.37(15)	83.44(10) / 87.61(15)
N4−Re1−N3	73.76(18)	74.33(15	N3−Re1−Br1	87.13(12)	86.19(11)/ 88.11(15)
C11−Re1−C12	89.3(3)	88.9(2)	C13−Re1−N4	93.5(2)	91.9(2) /92.8(10)
C11−Re1−N3	174.5(2)	173.56(19)	C13−Re1−N3	90.4(2)	93.6(2) /90.4(9)
C11−Re1−N4	101.3(2)	99.2(2)	C12−Re1−Br1	90.9(2)	92.13(16) /92.44(19)
C12−Re1−N4	95.6(3)	97.5(2)	C13−Re1−Br1	176.41(19)	175.2(2) /178.3(9)
C12−Re1−N3	169.3(3)	171.8(2)	C11−Re1−Br1	94.1(2)	96.22(16) / 92.3(2)

PART 1. NMR SPECTRA

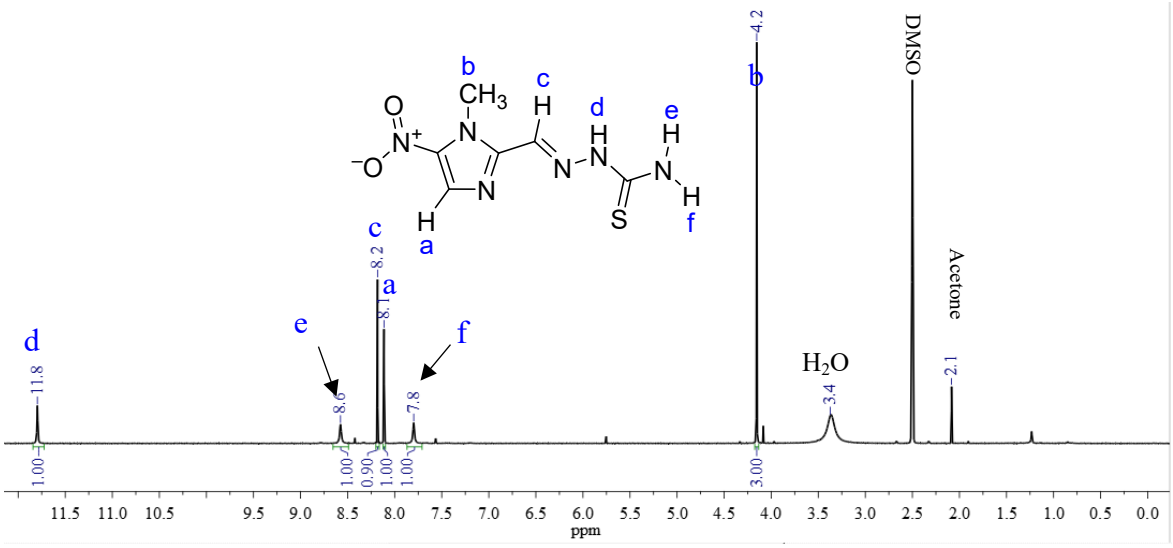

Figure S1.1– ^{1}H NMR (400 MHz) spectrum of Tsc^{H,H} in DMSO-d_6.

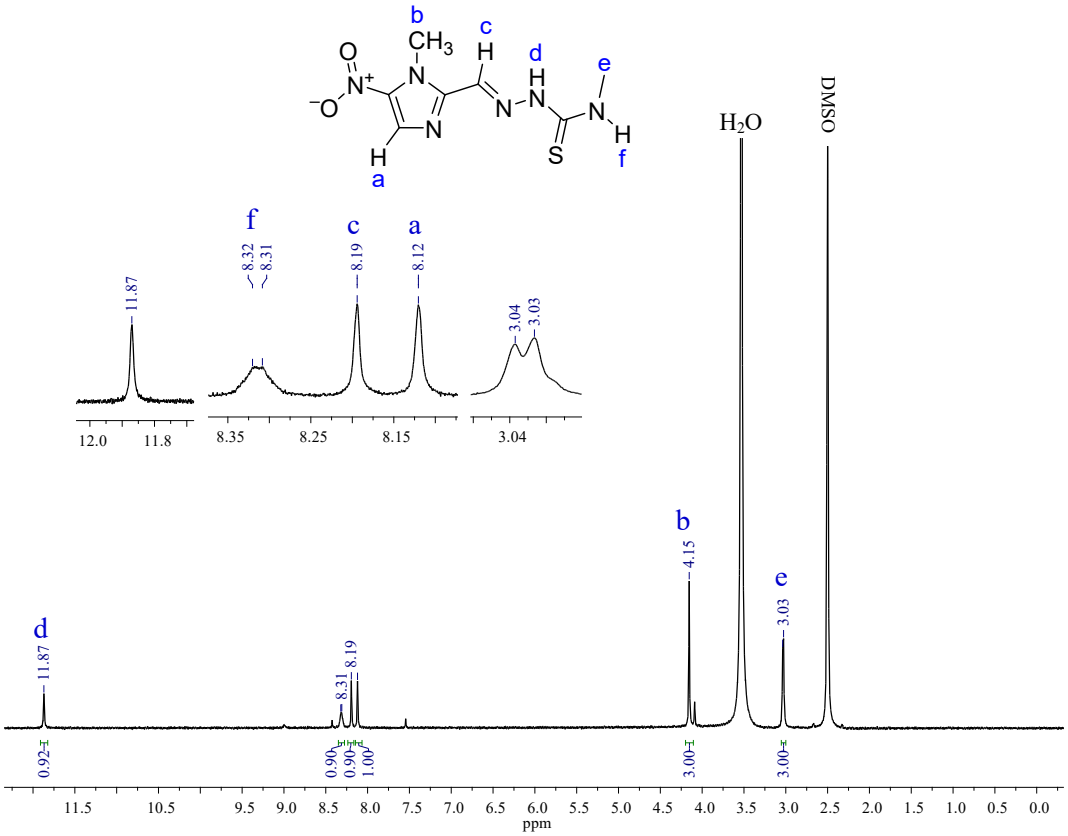

Figure S1.2 –^{1}H NMR (400 MHz) spectrum of Tsc^{H,Me} in DMSO-d_6.

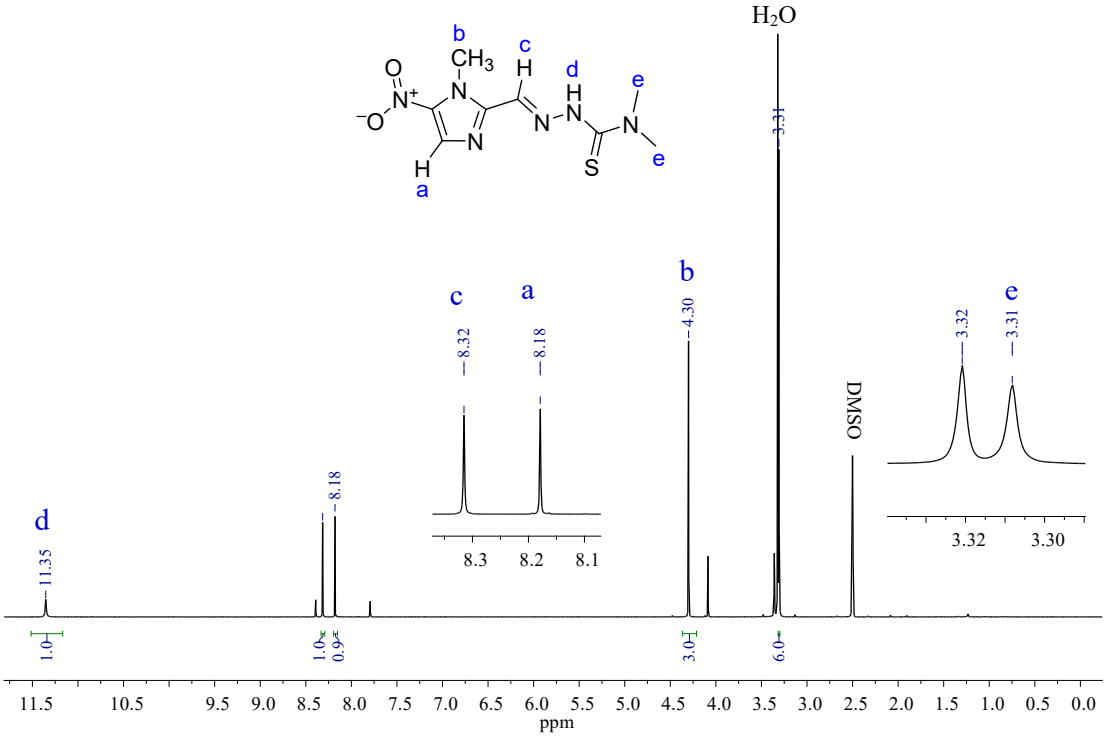

igure S1.3–^{1}H NMR (400 MHz) spectrum of Tsc^{Me,Me} in DMSO-d_6.

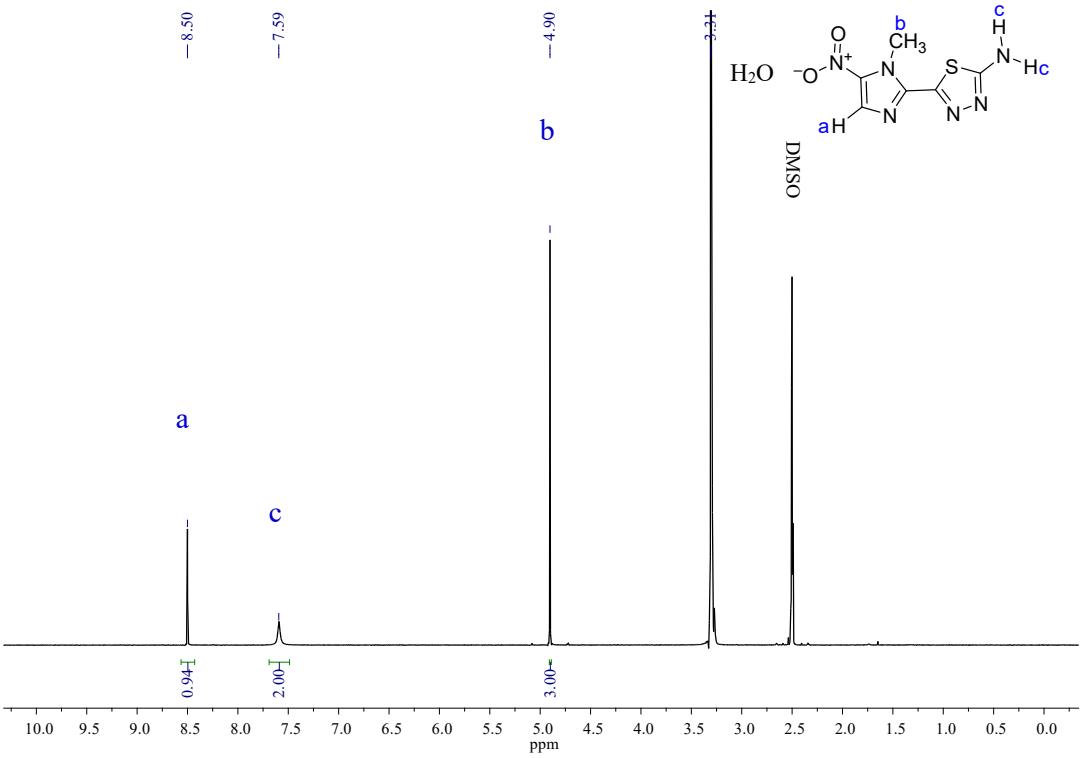

Figure S1.4 –^{1}H NMR (500 MHz) spectrum of L^{H,H} in DMSO-d_6.

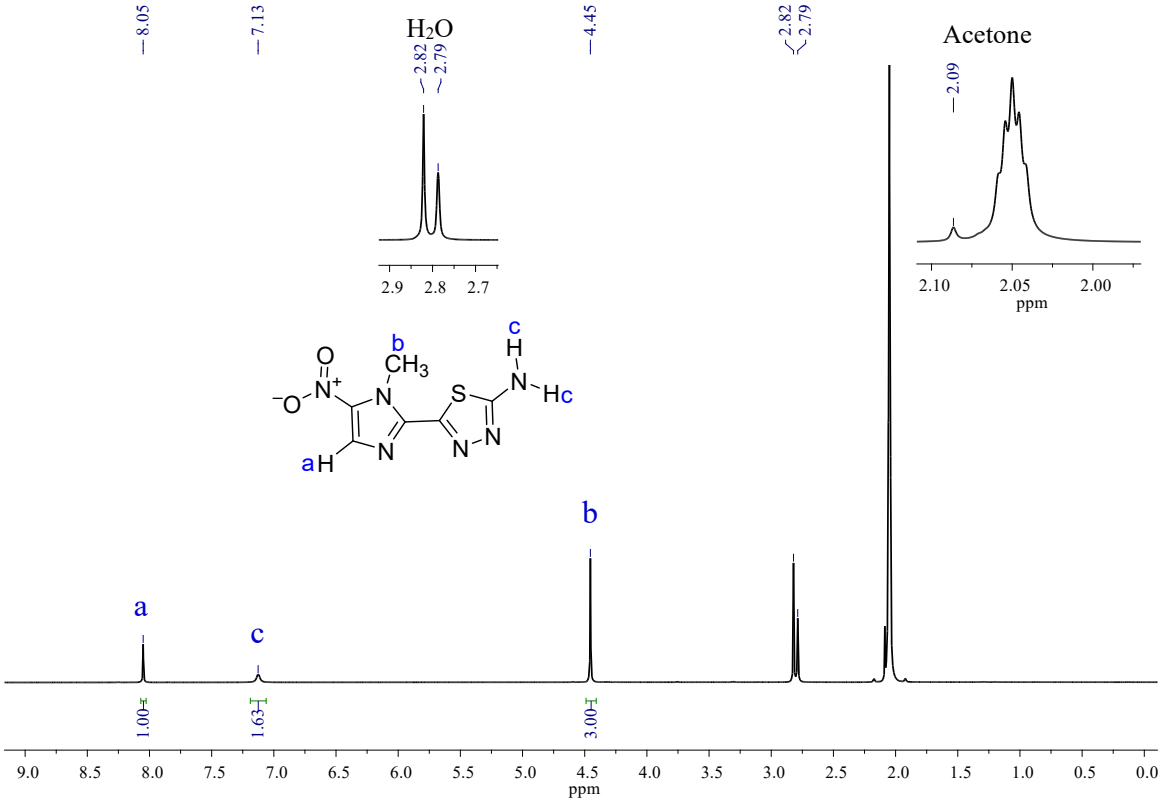

Figure S1.5 –^{1}H NMR (500 MHz) spectrum of $L^{H,H}$ in acetone-d_6 .

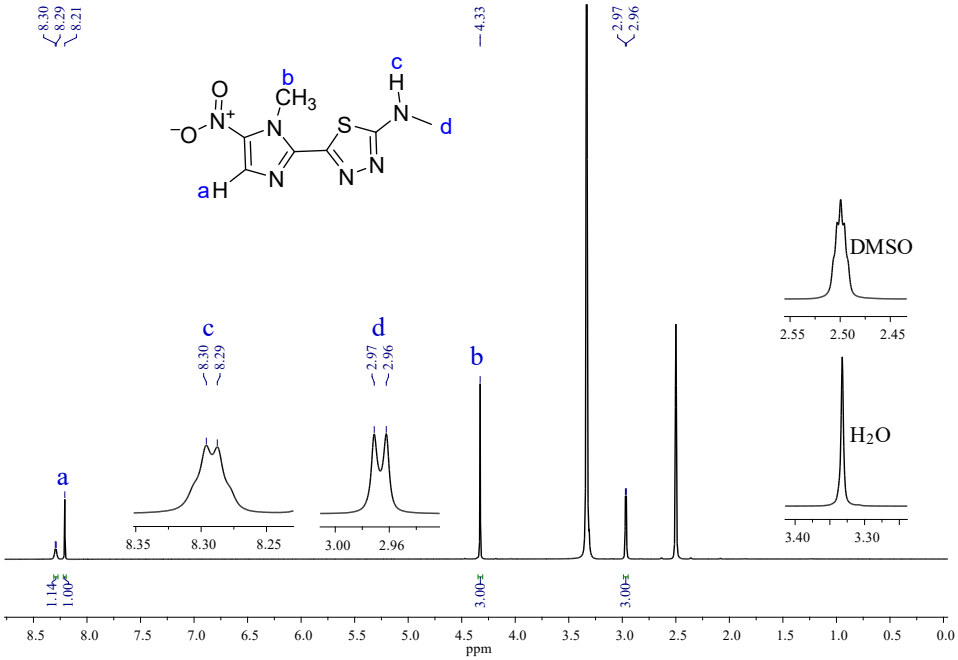

Figure S1.6 –^{1}H NMR (500 MHz) spectrum of $L^{H,Me}$ in DMSO-d_6.

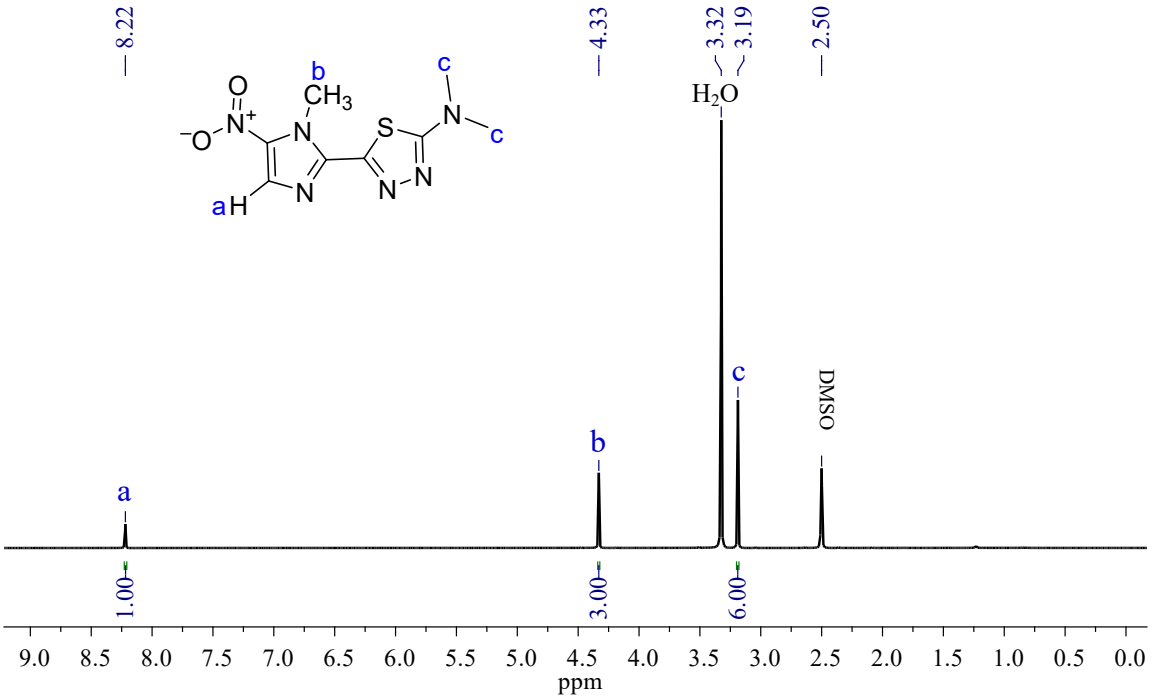

Figure S1.7 –^{1}H NMR (500 MHz) spectrum of $L^{Me,Me}$ in DMSO-d_6.

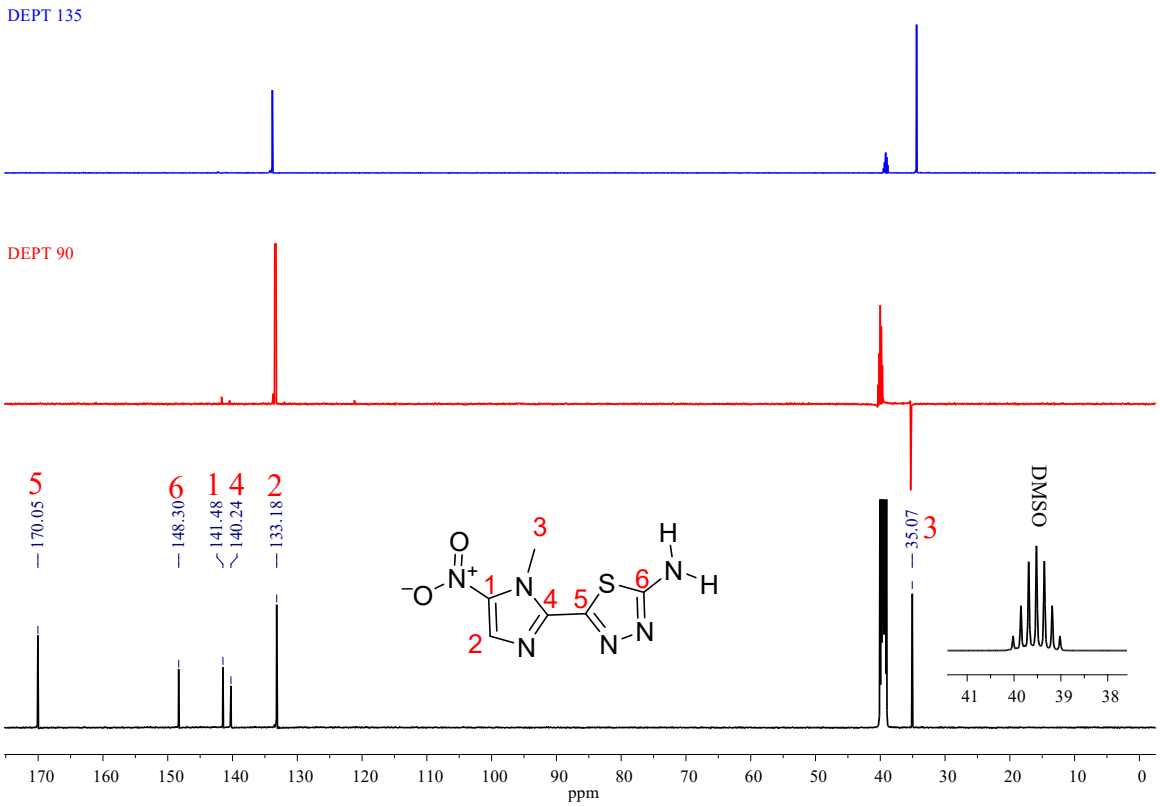

Figure S1.8 – DEPT and ^{13}C NMR spectra (125.8 MHz) of the compound $L^{H,H}$ in DMSO-d_6.

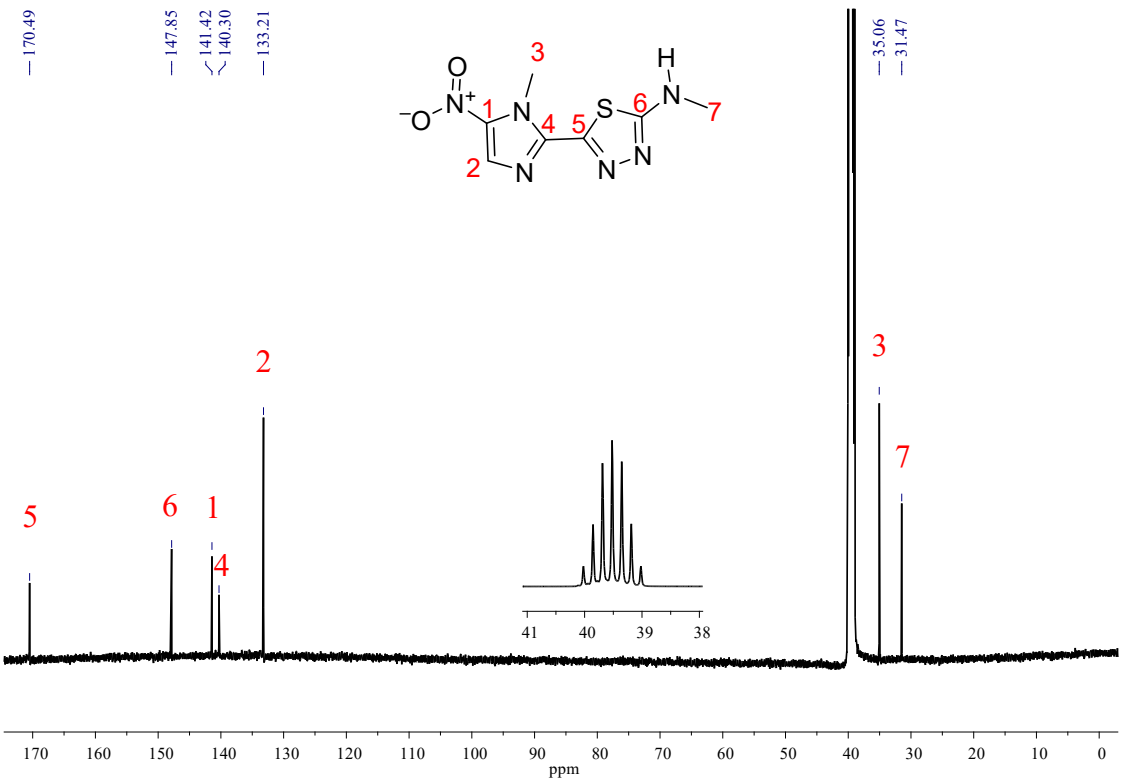

Figure S1.9 – ^{13}C NMR spectrum (125.8 MHz) of $L^{H,Me}$ in DMSO-d_6.

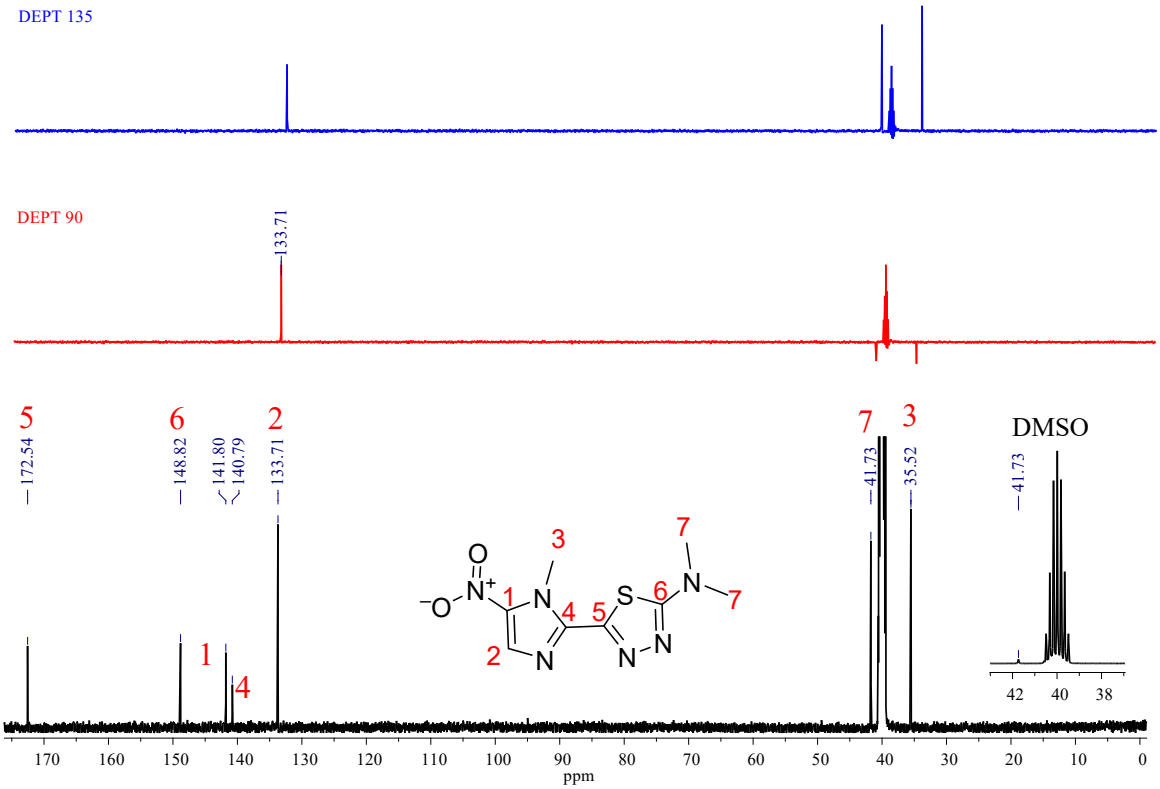

Figure S1.10 – DEPT and ^{13}C NMR (125.8 MHz) of $L^{Me,Me}$ in DMSO-d_6.

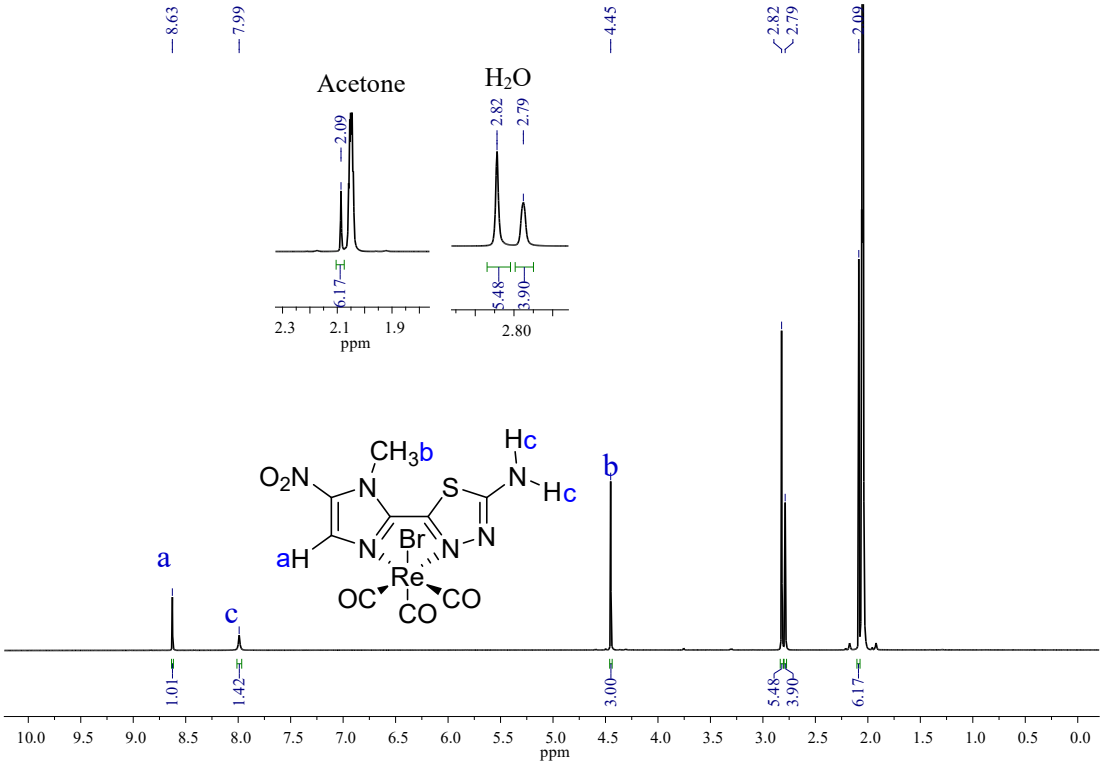

Figure S1.11 –^{1}H NMR (500 MHz) spectrum of [ReBr(CO)$_3$L^{H,H}] in acetone-d_6.

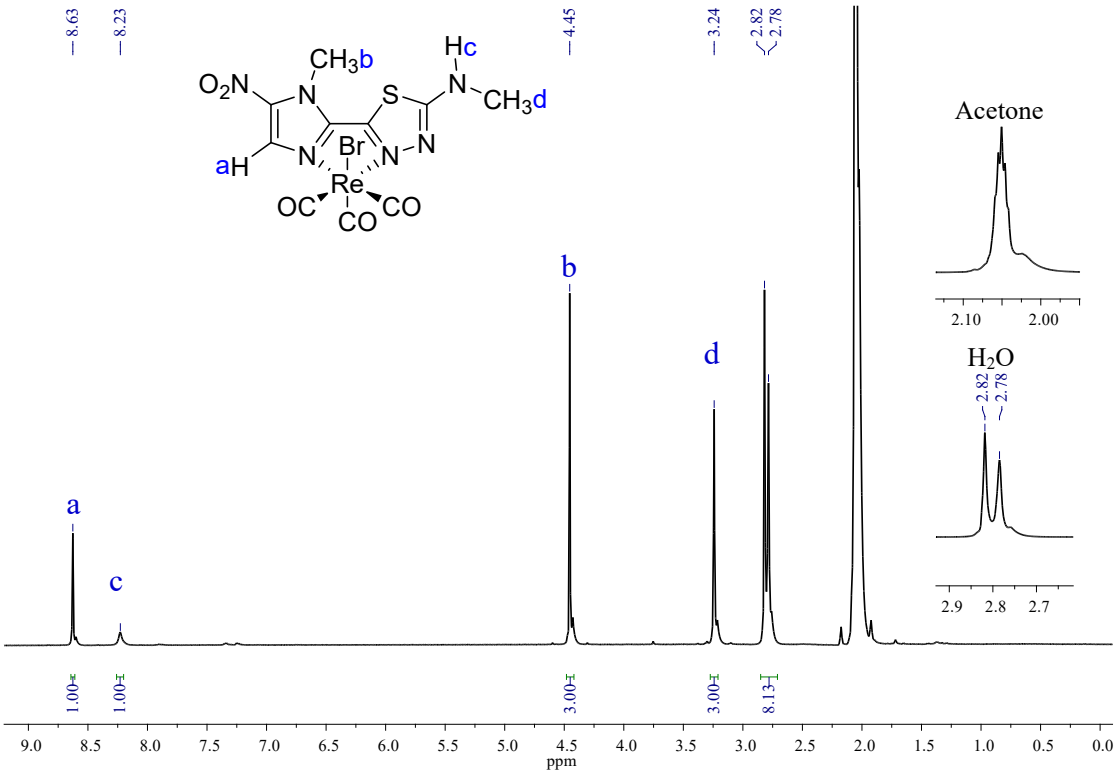

Figure S1.12 –^{1}H NMR (500 MHz) spectrum of [ReBr(CO)$_3$L^{H,Me}] in acetone-d_6.

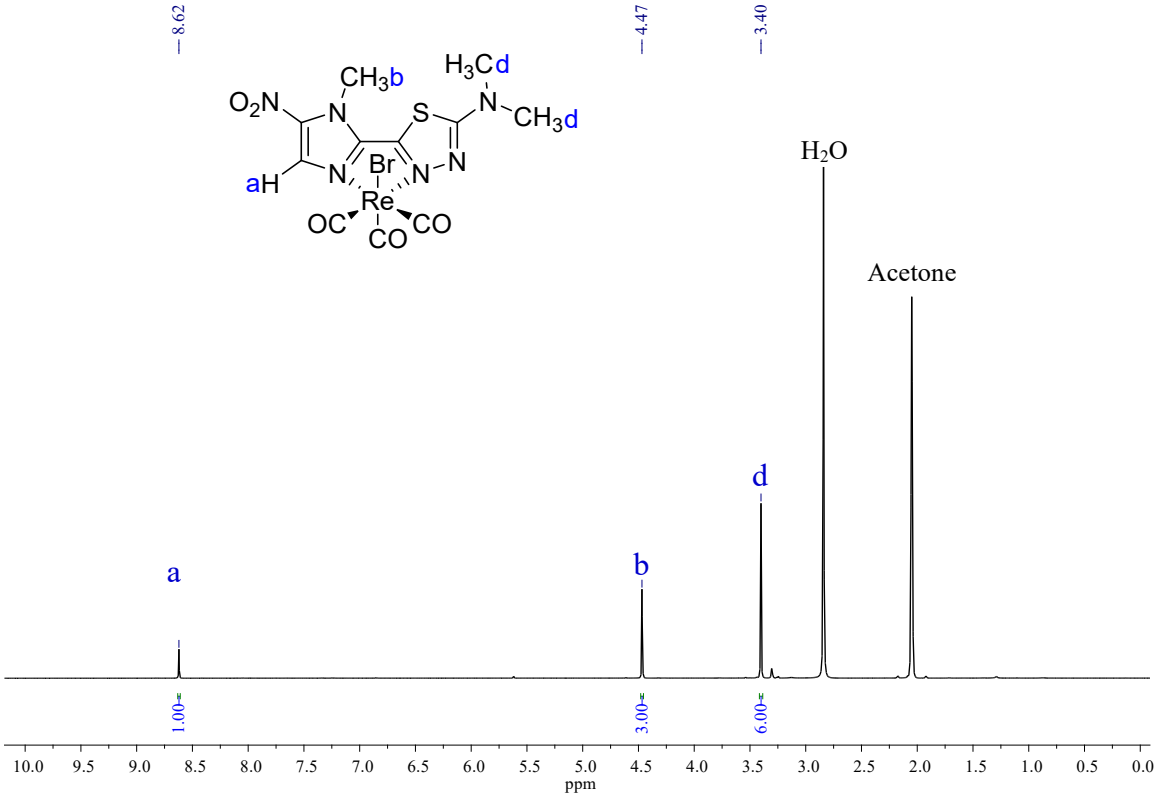

Figure S1.13 –^{1}H NMR (500 MHz) spectrum of [ReBr(CO)$_3$L^{Me,Me}] in acetone-d_6.

Figure S1.14 – DEPT and ^{13}C NMR (125.8 MHz) spectra of $[ReBr(CO)_3L^{H,H}]$ in acetone-d_6.

Figure S1.15 –DEPT and ^{13}C NMR (125.8 MHz) spectra of $[ReBr(CO)_3L^{H,Me}]$ in acetone-d_6.

Figure S1.16 –DEPT and ^{13}C RMN (125.8 MHz) spectra of $[ReBr(CO)_3L^{Me,Me}]$ in acetone-d_6.

PART 2. Infrared spectroscopy.

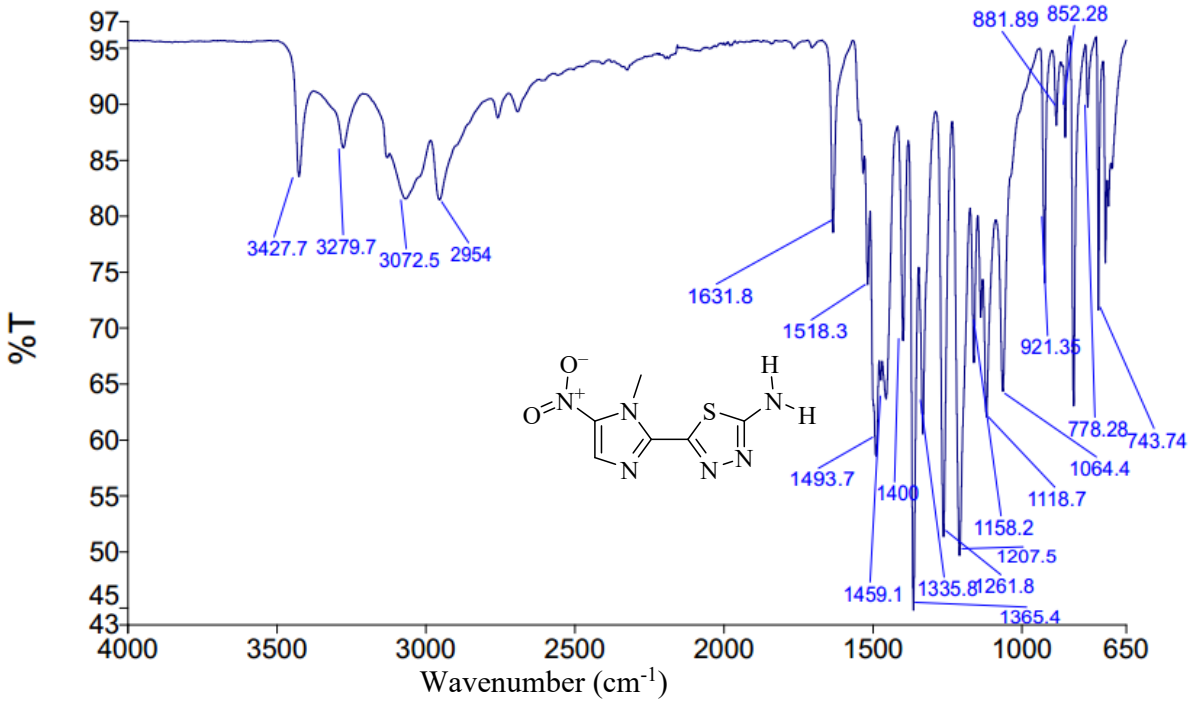

Figure S2.1 – Infrared spectrum of $L^{H,H}$.

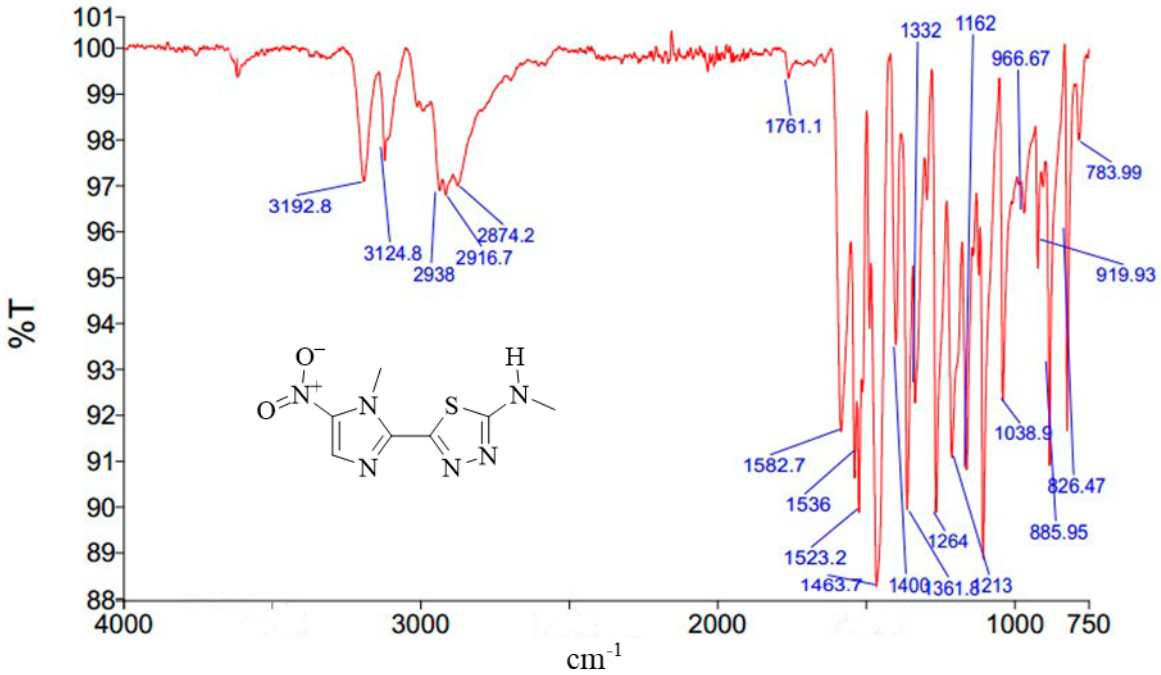

Figure S2.2 – Infrared spectrum of $L^{H,Me}$.

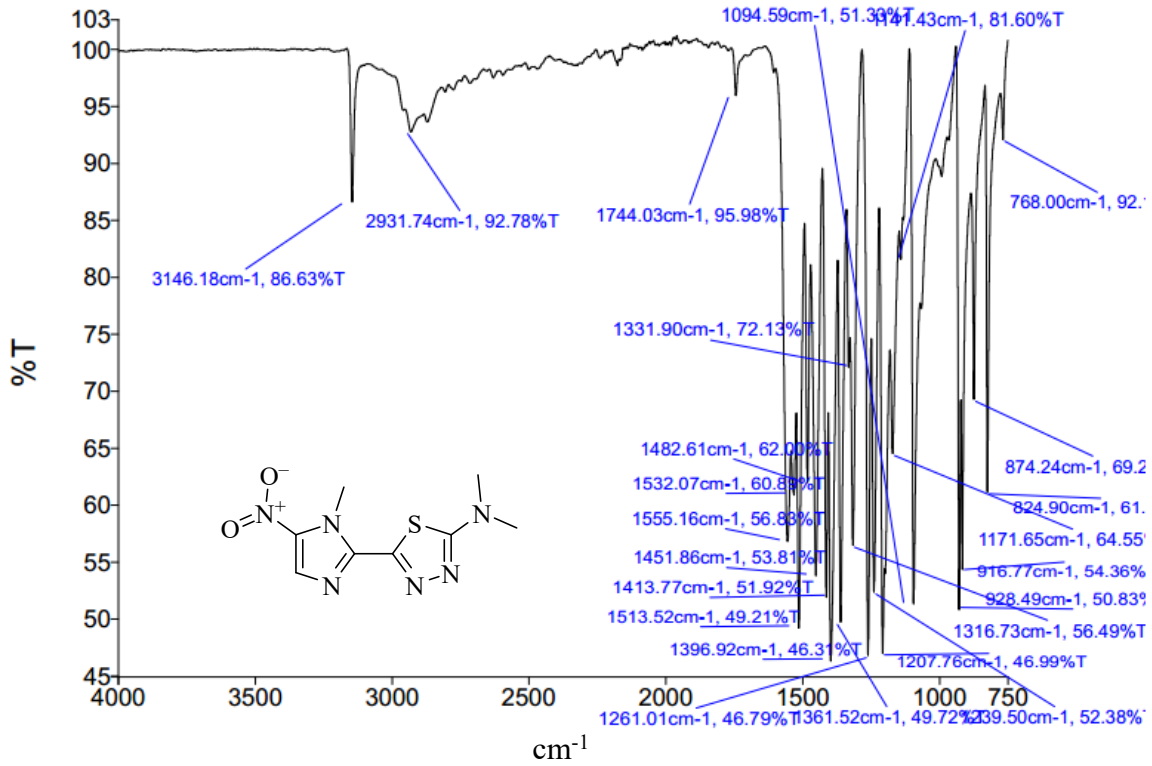

Figure S2.3 – Infrared spectrum of $L^{Me,Me}$.

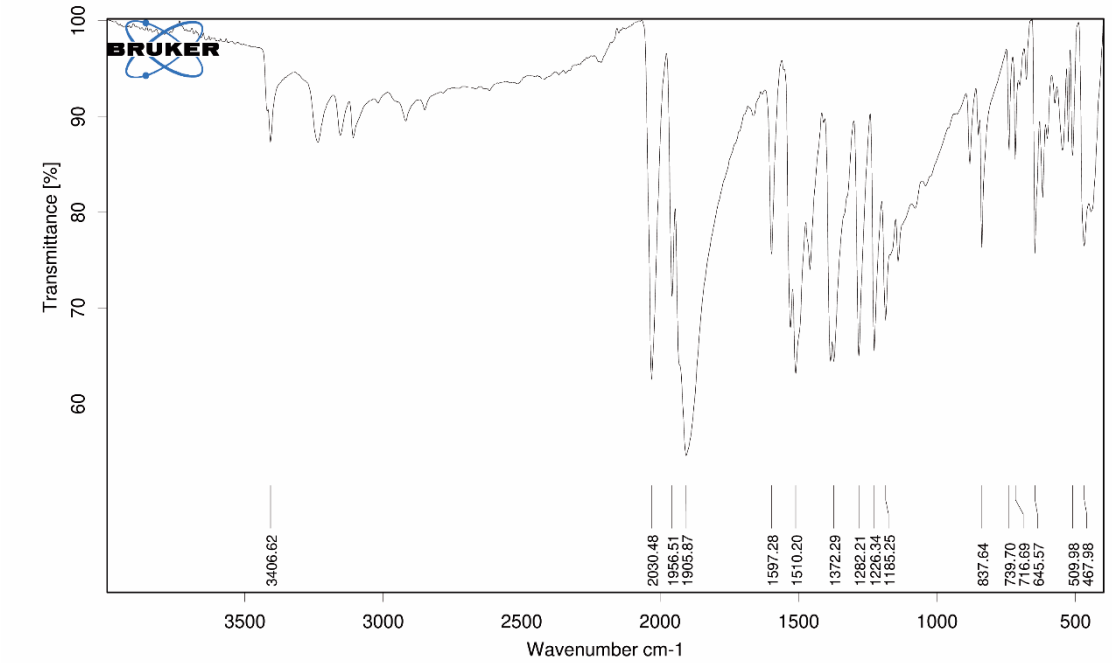

Figure S2.4- IR spectrum of $[ReBr(CO)_3L^{H,H}]$ (**1**).

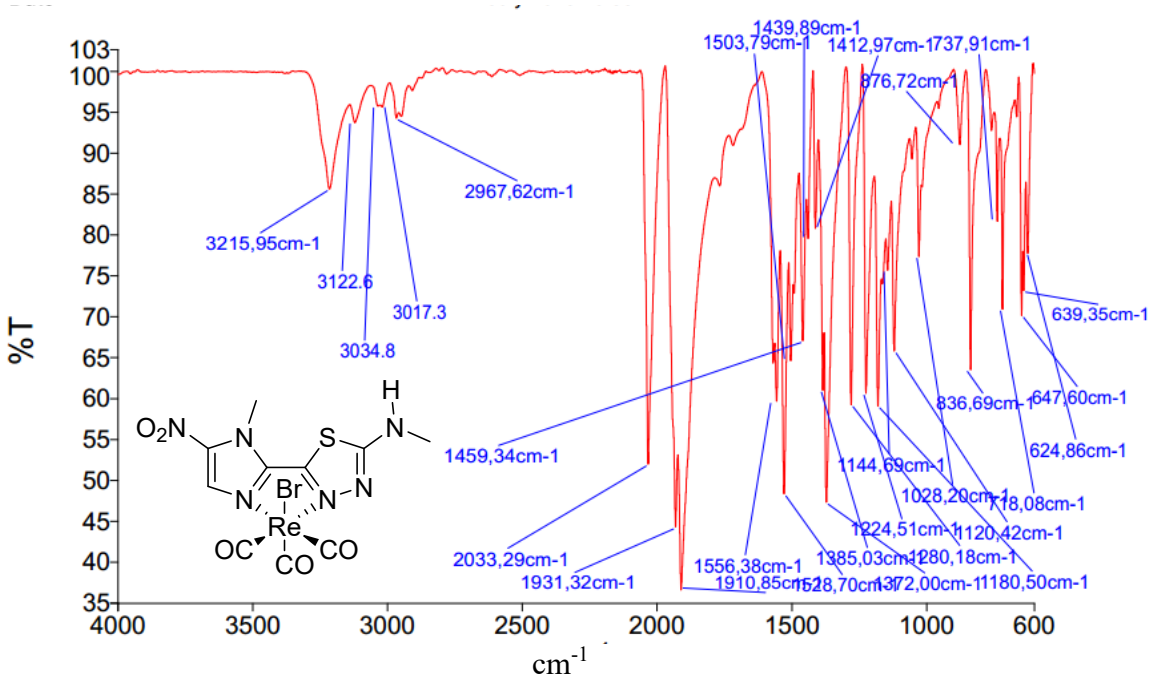

Figure S2.5- IR spectrum of [ReBr(CO)$_3$L^{H,Me}] (**2**).

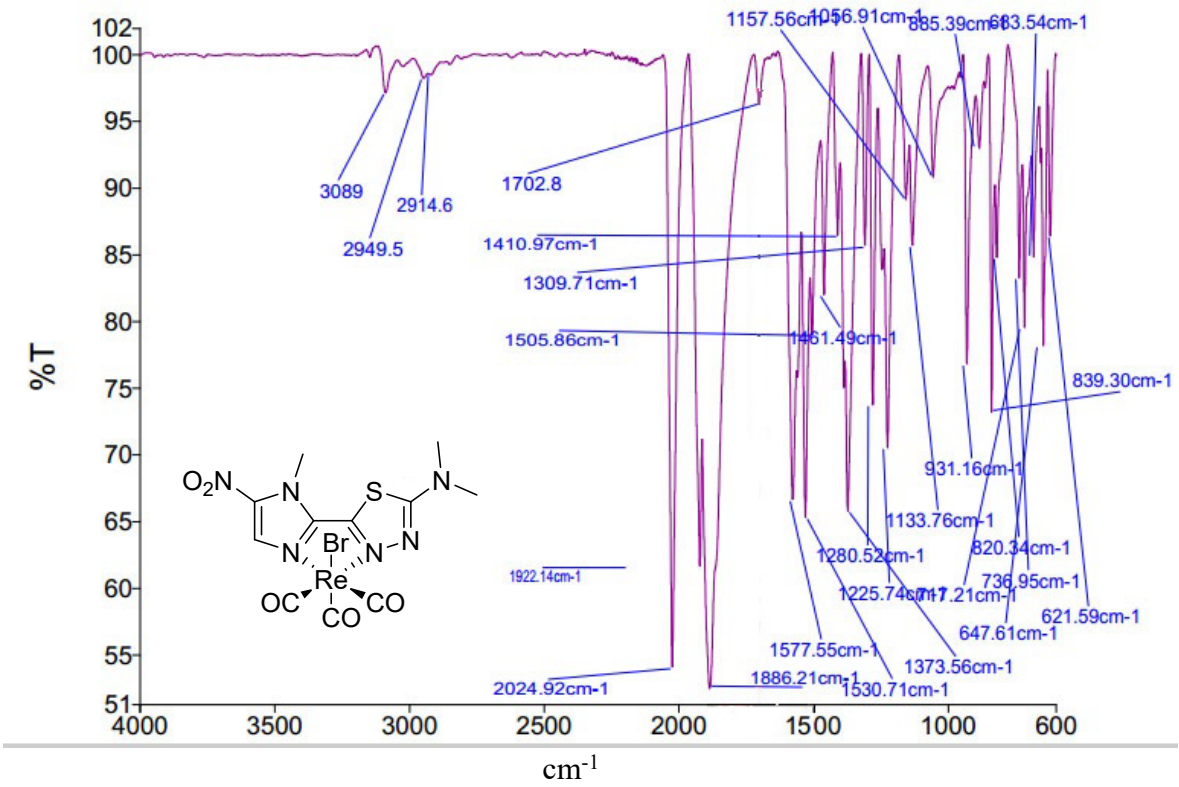

Figure S2.6- IR spectrum of [ReBr(CO)$_3$L^{Me,Me}] (**3**).

PART 3. Mass spectrometry

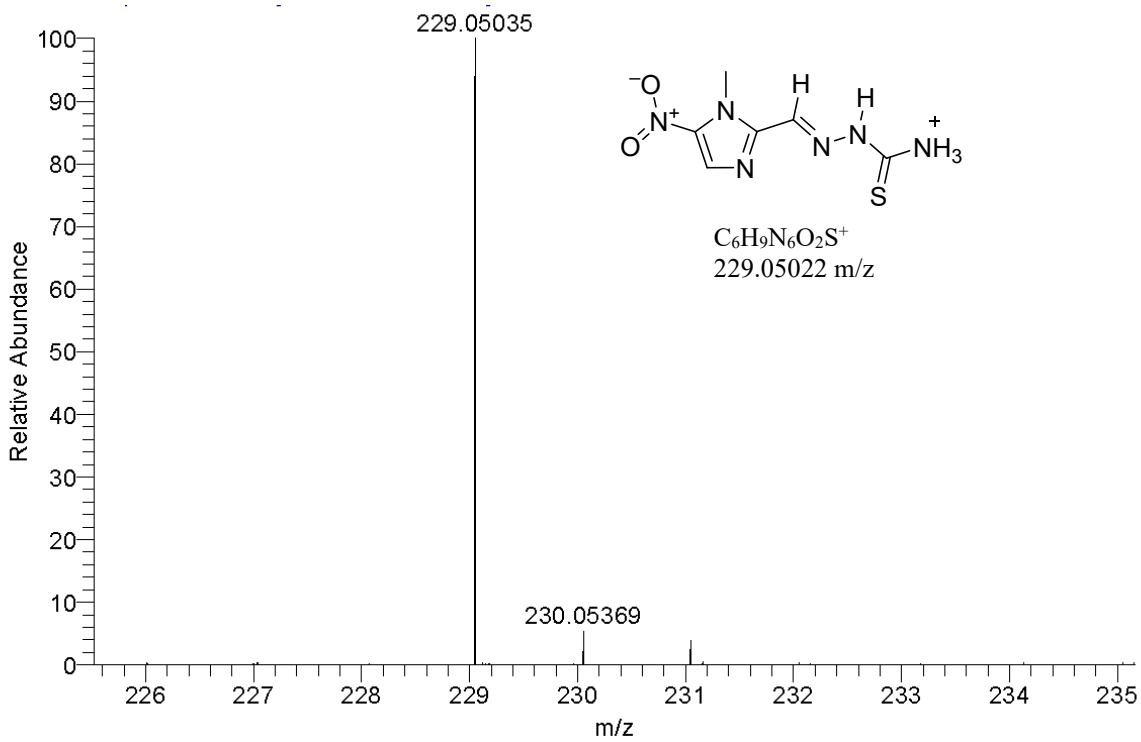

Figure S3.1 –HR-ESI-MS(+) spectrum of **Tsc^{H,H}**.

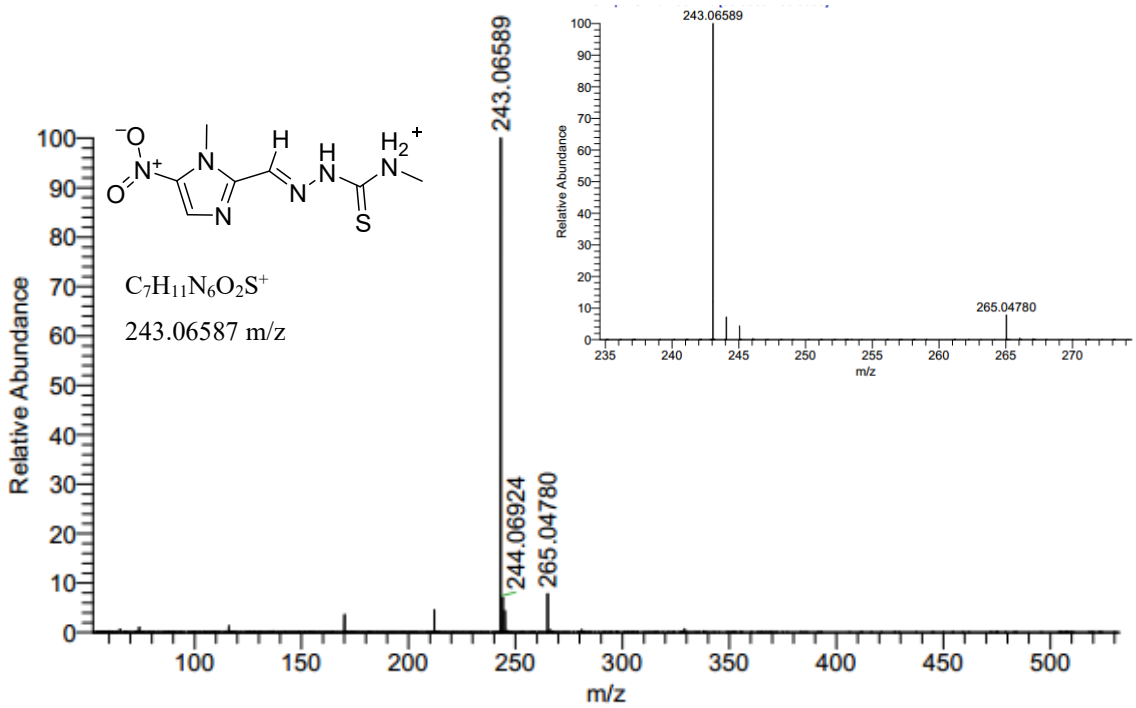

Figure S3.2 –HR-ESI-MS(+) spectrum of Tsc^{Me,H}.

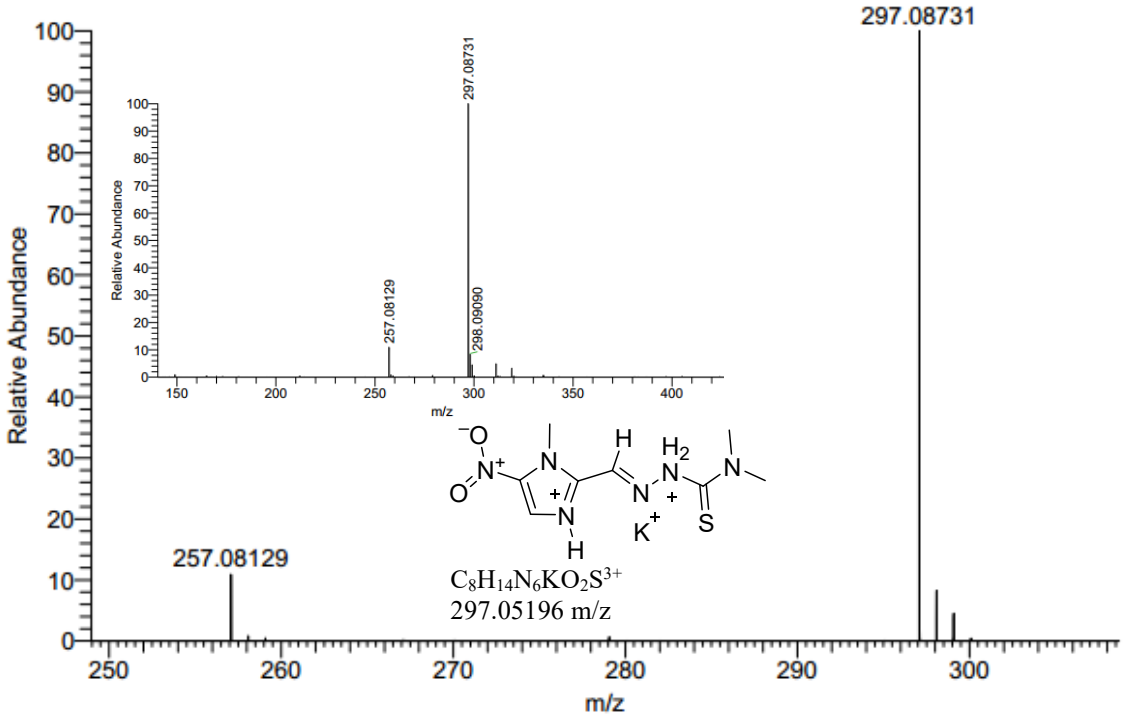

Figure S3.3–HR-ESI-MS(+) spectrum T**sc**^{Me,Me}.

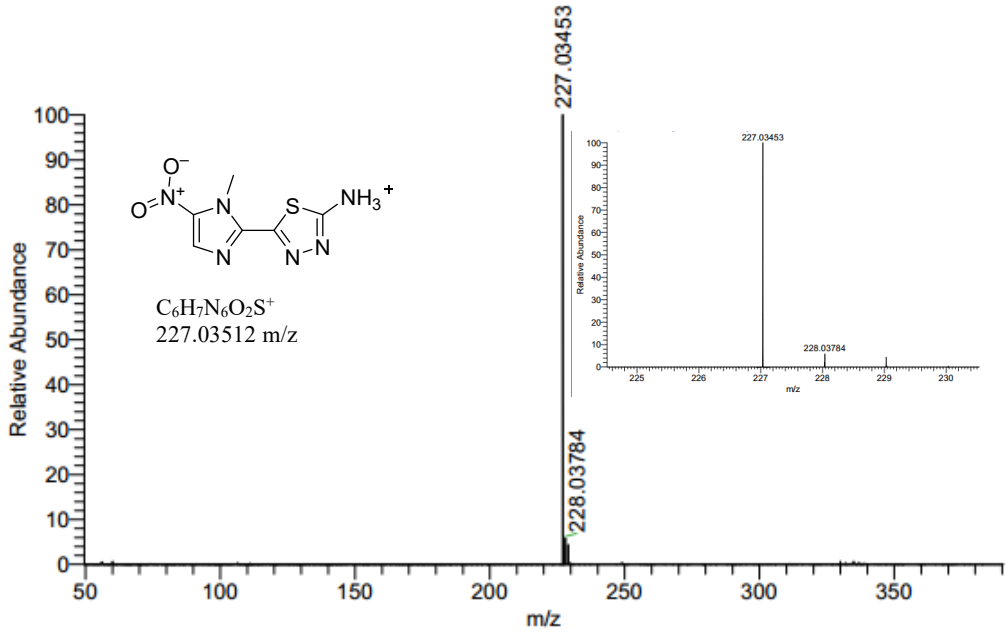

Figure S3.4 –HR-ESI-MS(+) spectrum of $L^{H,H}$.

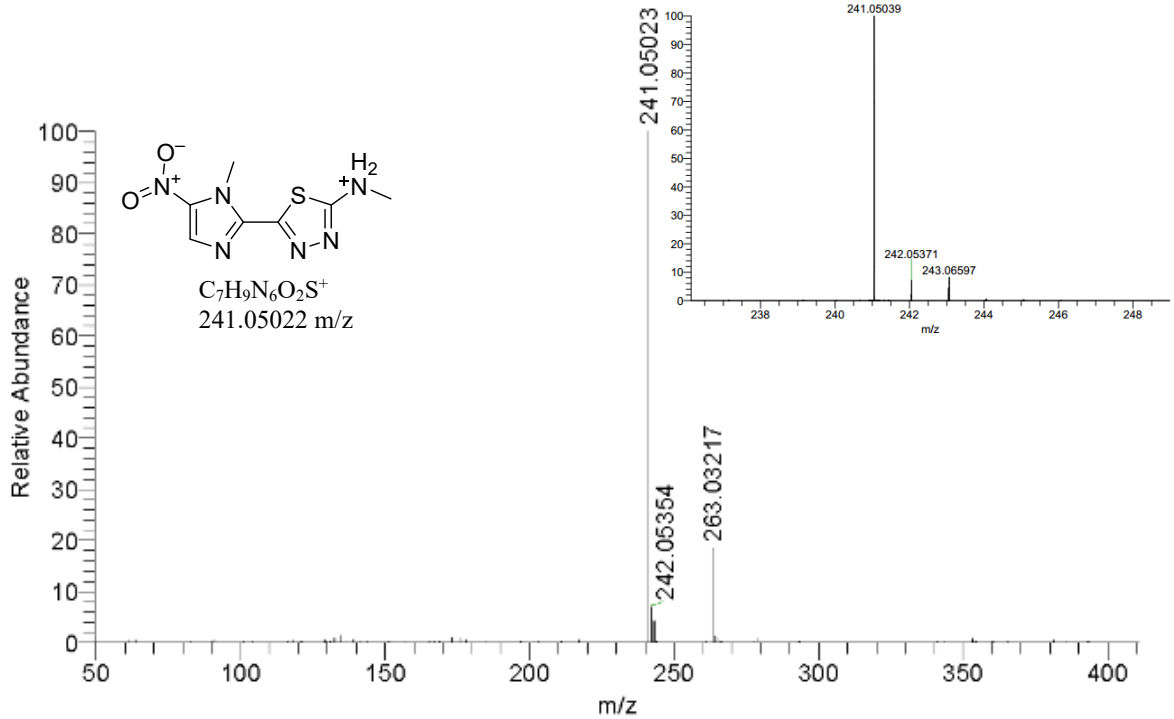

Figure S3.5 –HR-ESI-MS(+) spectrum of $L^{H,Me}$.

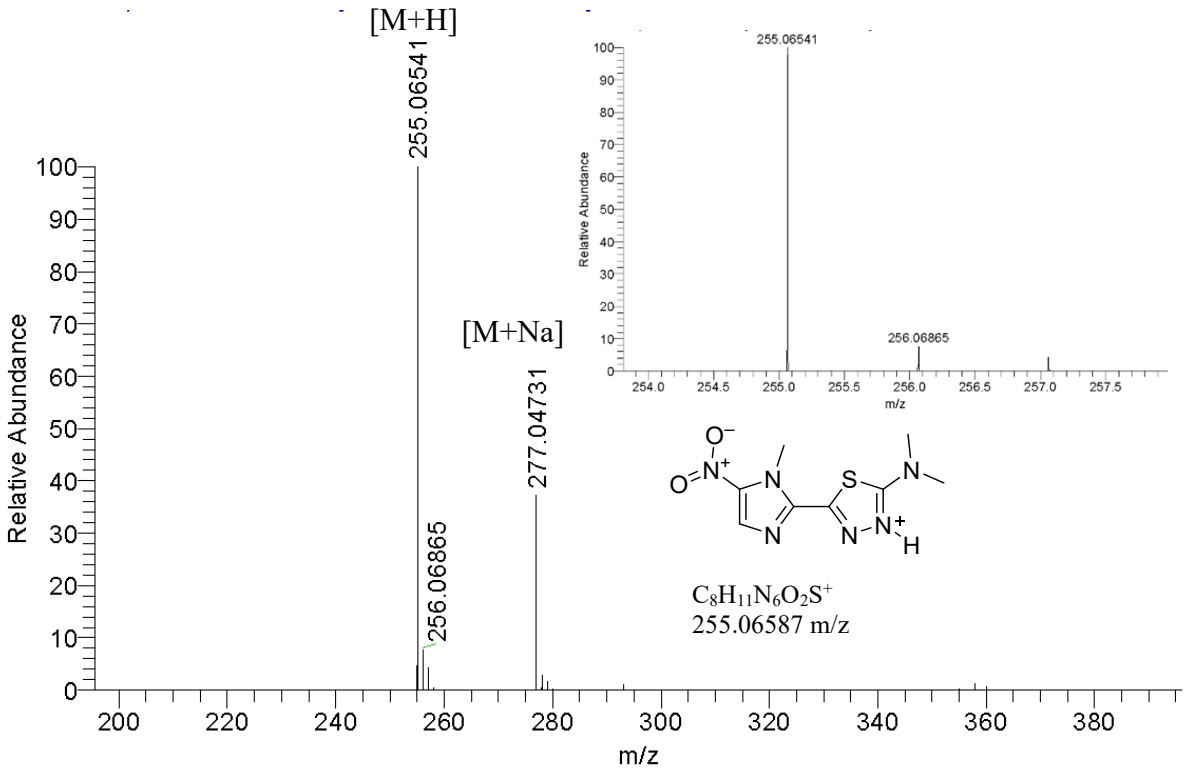

Figure S3.6 –HR-ESI-MS(+) spectrum of $L^{Me,Me}$.

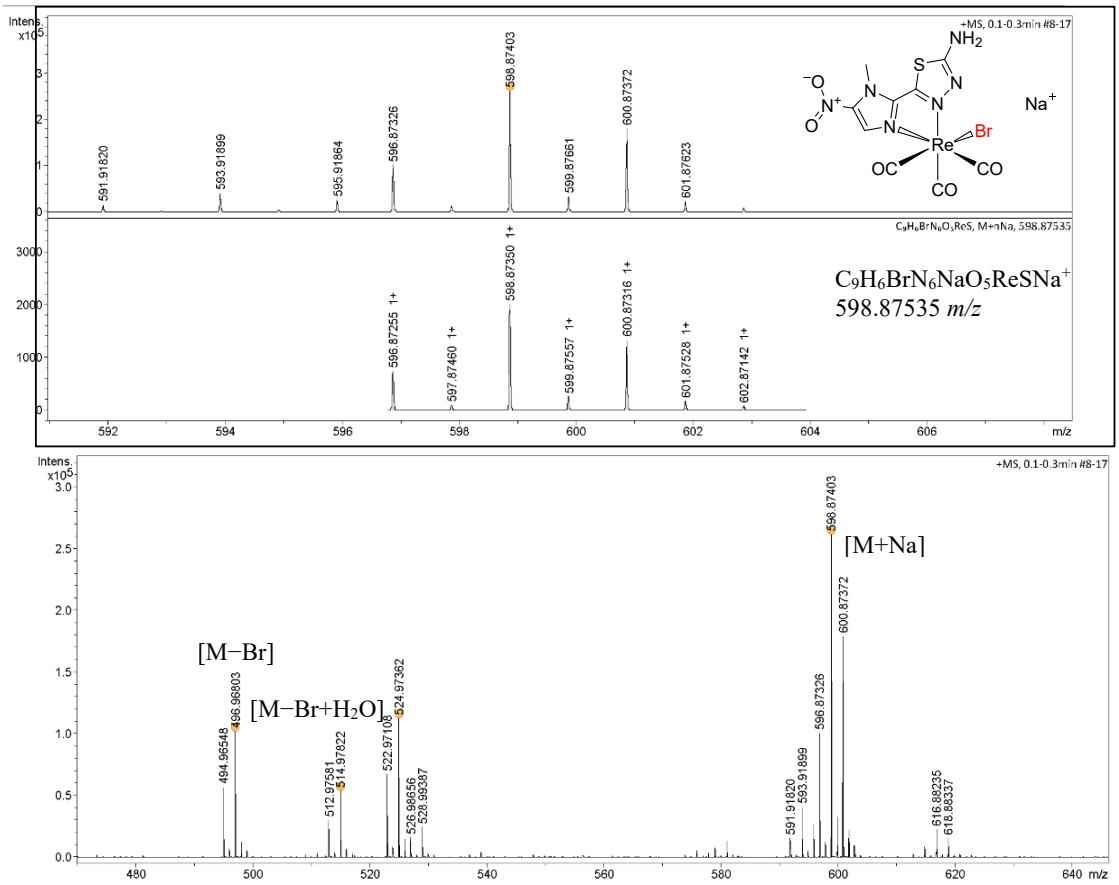

Figure S3.7 –HR-ESI-MS(+) spectrum of [ReBr(CO)$_3$L^{H,H}].

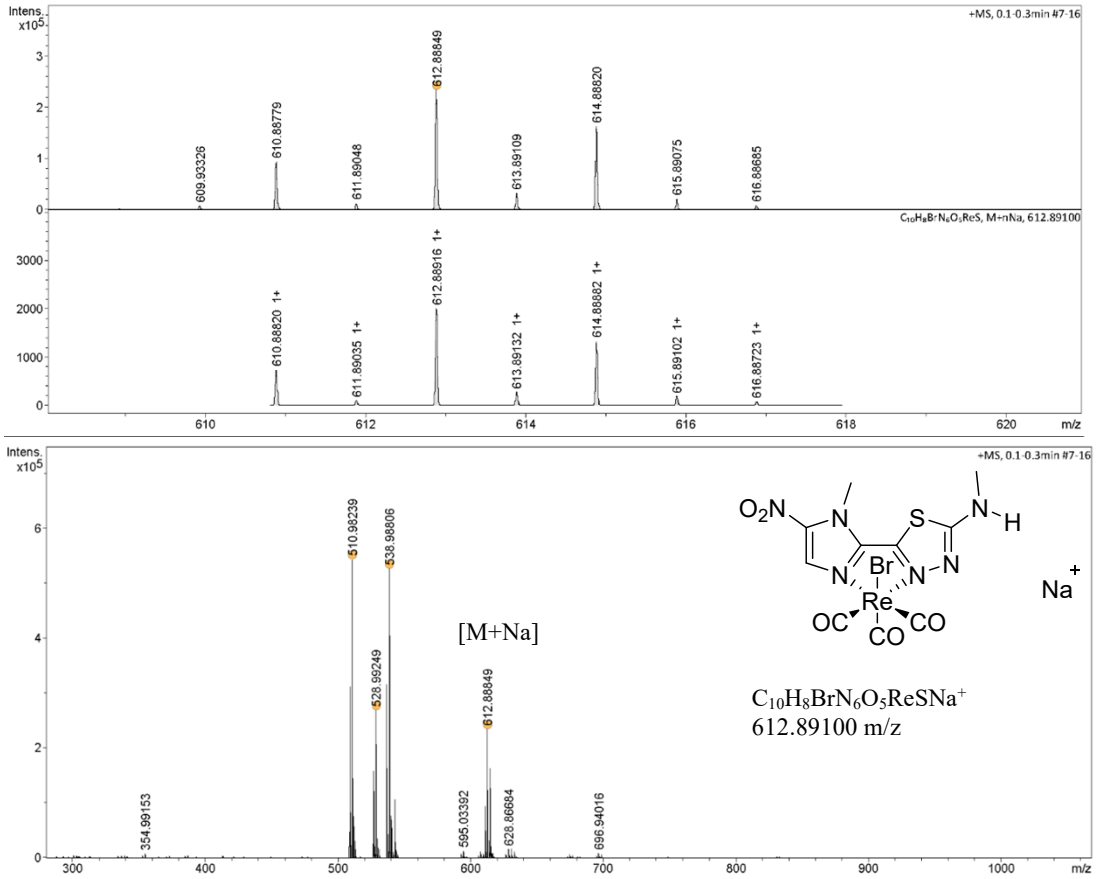

Figure S3.8 –HR-ESI-MS(+) spectrum of [ReBr(CO)$_3$L^{H,Me}].

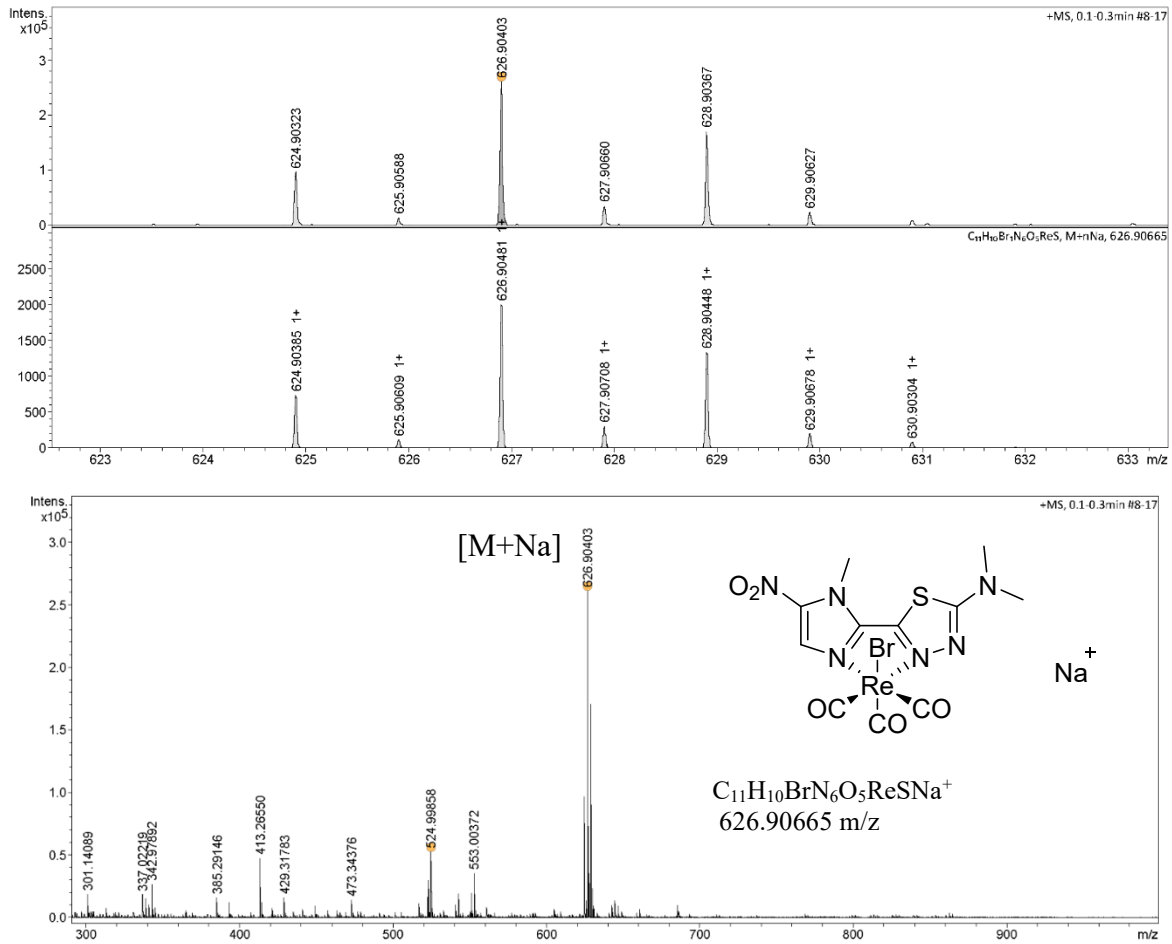

Figure S3.9 –HR-ESI-MS(+) spectrum of [ReBr(CO)$_3$L^{Me,Me}].

PART 4. Crystallographic data

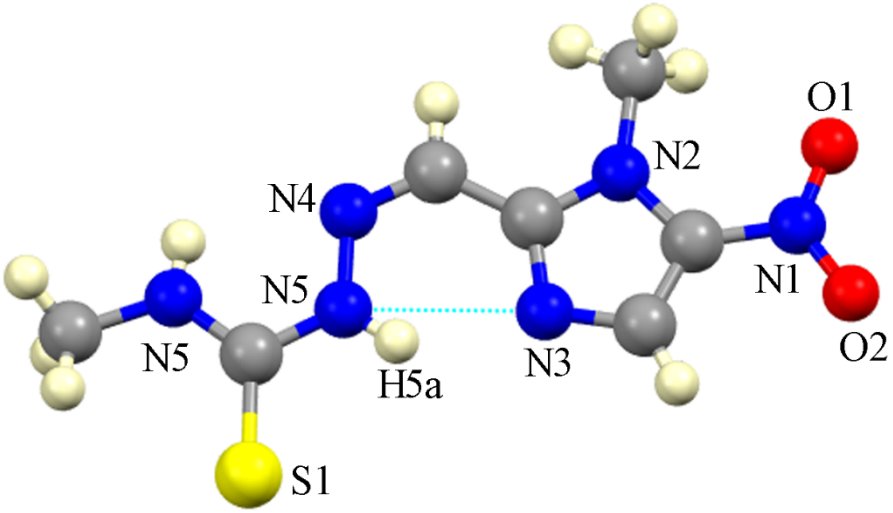

Figure S4.1 Intramolecular hydrogen bonds involved in the crystal structure of $Tsc^{H,Me}$. [N(5)···N(3) = 2.6973(14) Å, N(5)−H(a)···N(3) = 135.3(14) °].

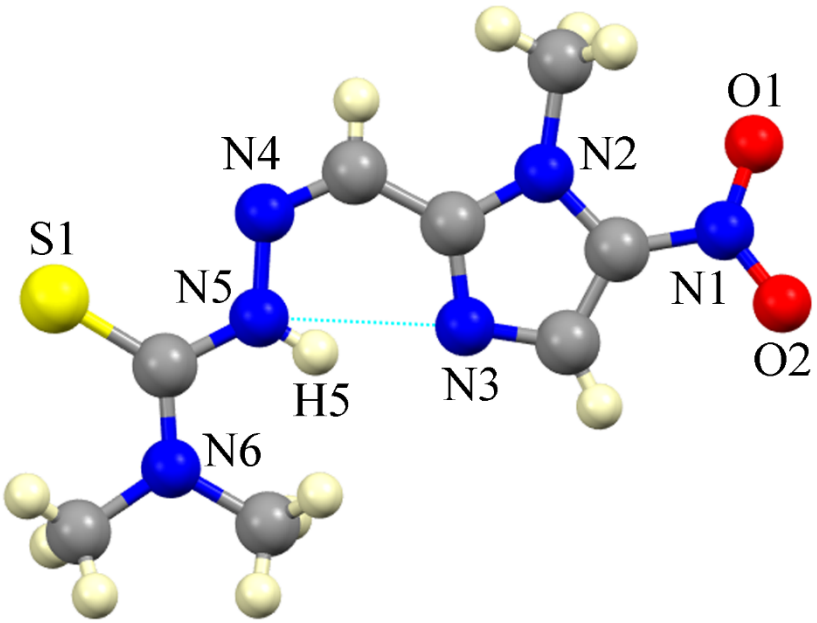

Figure S4.2 Intramolecular hydrogen bond involved in the crystal structure of the compound $Tsc^{Me,Me}$. [N(5)···N(3) = 2.6994(17) Å, N(5)−H(a)···N(3) = 138.7(16) °].

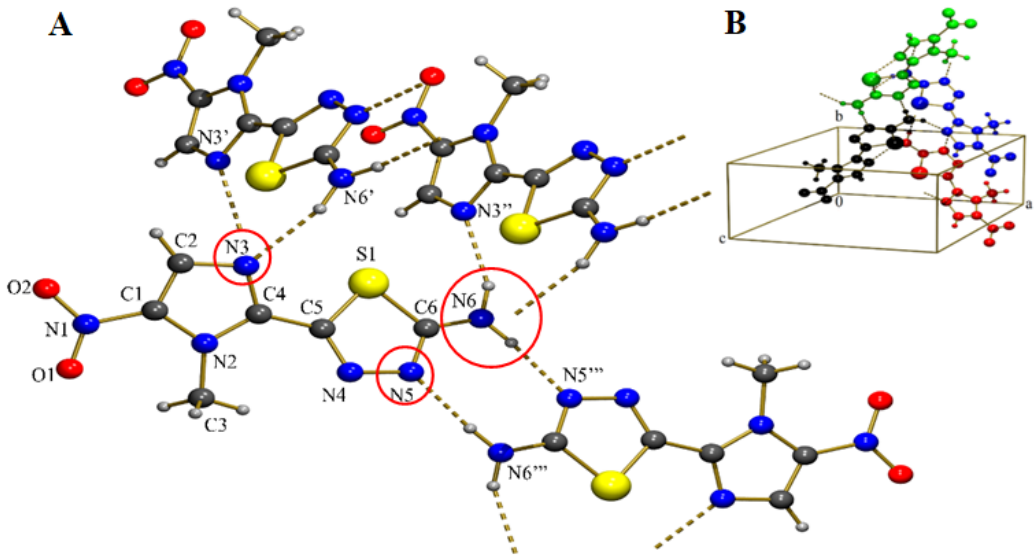

Figure S4.3 – (A) Intermolecular hydrogen bonds involved in the crystal structure of the compound $L^{H,H}$. The hydrogen donor group N(6)–H(6) and the hydrogen receptor atoms N(3) and N(5) that form the hydrogen bonds are in red circle. (B) – Central black molecule forming hydrogen bonds with the red, blue and green molecules generated by symmetry. [N(6)···N(3) = 3.026(4) Å, N(6)–H(a)···N(3) = 156(4) °]; [N(6)···N(5) = 2.924(4) Å, N(6)–H(b)···N(5) = 172(3) °]. Symmetry operations: (a) 1-x, -1/2+y, 3/2-z and (b) 1-x, -1-y, 1-z.

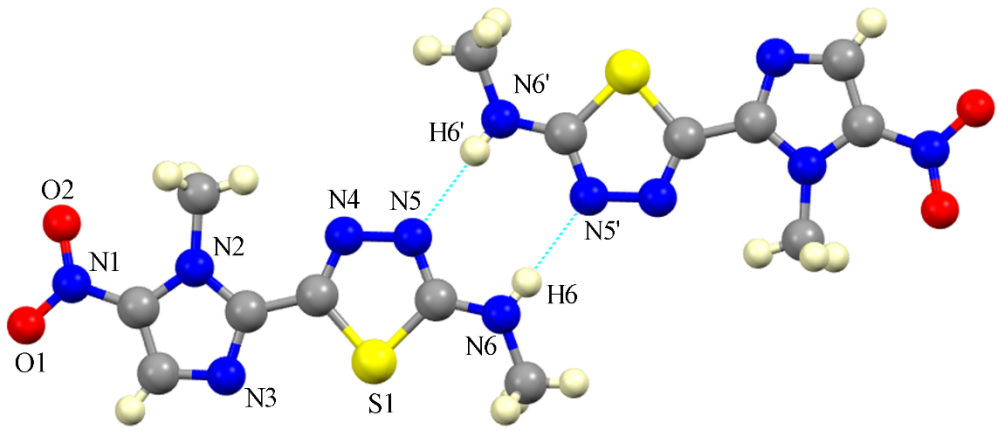

Figure S4.4 Intermolecular hydrogen bonds involved in the crystal structure of the compound $L^{H,Me}$. [N(6)···N(3) = 2.938(3) Å, N(6)–H(a)···N(3) = 174(3) °]. Symmetry operation: (′) 1/2-x, -1/2+y, 1/2-z.

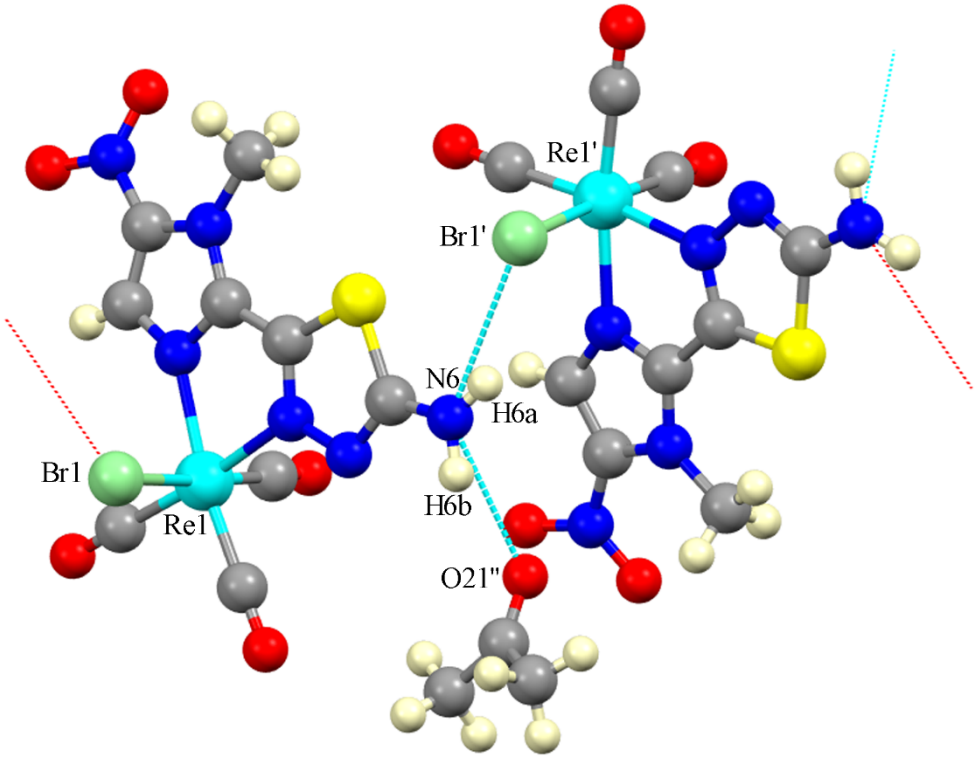

Figure S4.5 Intermolecular hydrogen bonds involved in the crystal structure of [ReBr(CO)$_3$L^{H,H}] (**1**). [N(6)···Br(1′) = 3.319(6) Å, N(6)–H(a)···Br(1′) = 147(10) °] and [N(6)···O(21′′) = 2.983(9)Å, N(6)–H(b)···O(21′′) = 147(15) °]. Symmetry operations: (′) 1/2+x, 1-y, +z; (′′)1/2+x, -y, +z.

PART 5 Biological studies

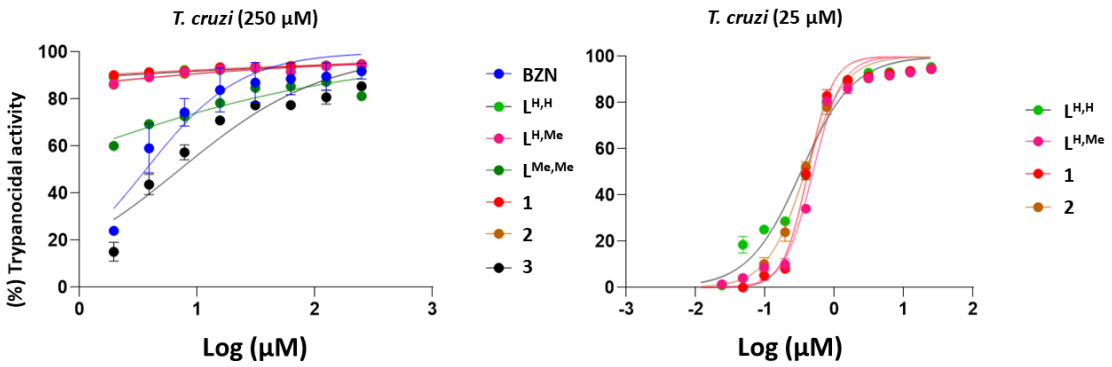

Figure S5.1 – Percentage of trypanocidal activity at different concentrations for the compounds benznidazole (Bz), $L^{H,H}$, $L^{H,Me}$, $L^{Me,Me}$, $[ReBr(CO)_3L^{H,H}]$ (**1**), $[ReBr(CO)_3L^{Me,H}]$ (**2**) and $[ReBr(CO)_3L^{Me,Me}]$ (**3**) against the Tulahuen strain of *T. cruzi*. The graph on the left represents the experiment with the initial concentration of the compounds 250 µM. The graph on the right represents the experiment with the initial concentration of the 25 µM compounds.

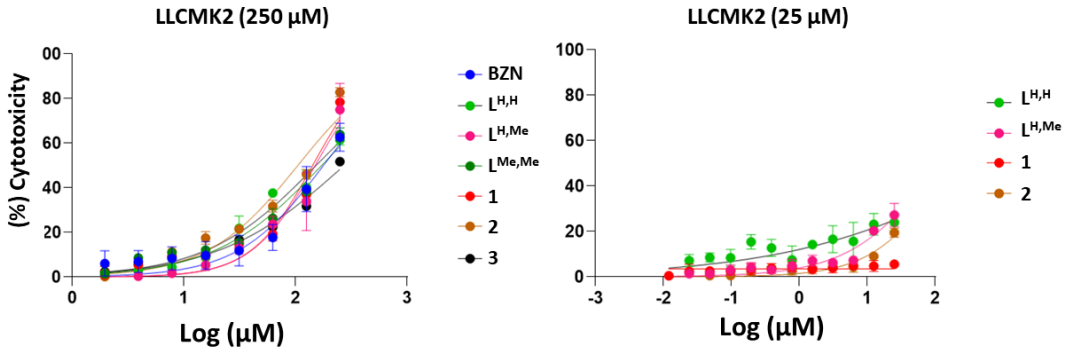

Figure S5.2 – Percentage of cytotoxicity at different concentrations for the compounds benznidazol (Bz), $L^{H,H}$, $L^{H,Me}$, $L^{Me,Me}$, $[ReBr(CO)_3L^{H,H}]$ (**1**), $[ReBr(CO)_3L^{Me,H}]$ (**2**) and $[ReBr(CO)_3L^{Me,Me}]$ (**3**) versus the Tulahuen strain of *T. cruzi*. The graph on the left represents the experiment with the initial concentration of the compounds 250 µM. The graph on the right represents the experiment with the initial concentration of the 25 µM compounds.

PART 6. Interaction studies with TcOYE

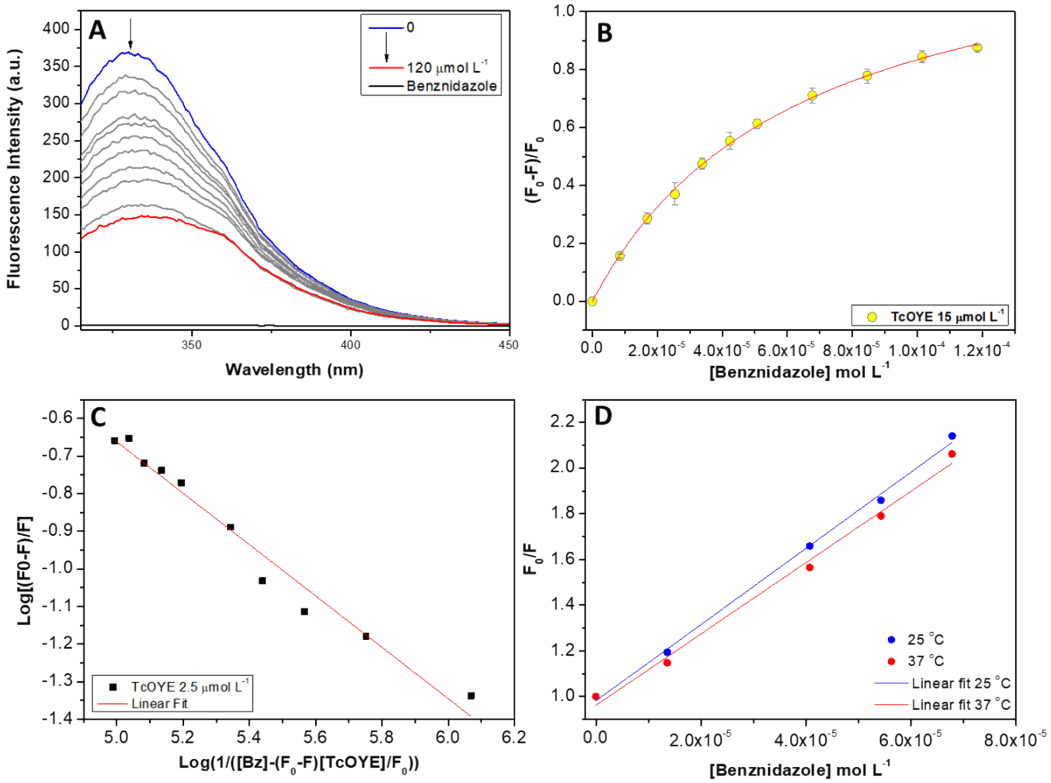

Figure S6.1 - (A) Fluorescence emission spectra (λ_{ex} = 295 nm) of the protein TcOYE at concentration of 15 μmol L^{-1} in the presence of increasing concentrations of benznidazole. (B) Variation of the intensities of the maximum fluorescence (λ_{max} = 336 nm) and non-linear fit to the Hill equation (Equation 1). (C) Logarithmic relationship for obtaining the number of linking sites according to Equation 2. Stern-Volmer plot at temperatures 25 and 37 °C. The spectra were obtained in Tris-HCl, pH 8.0; 100 mmol L^{-1} of NaCl and 2.5 % of DMSO.

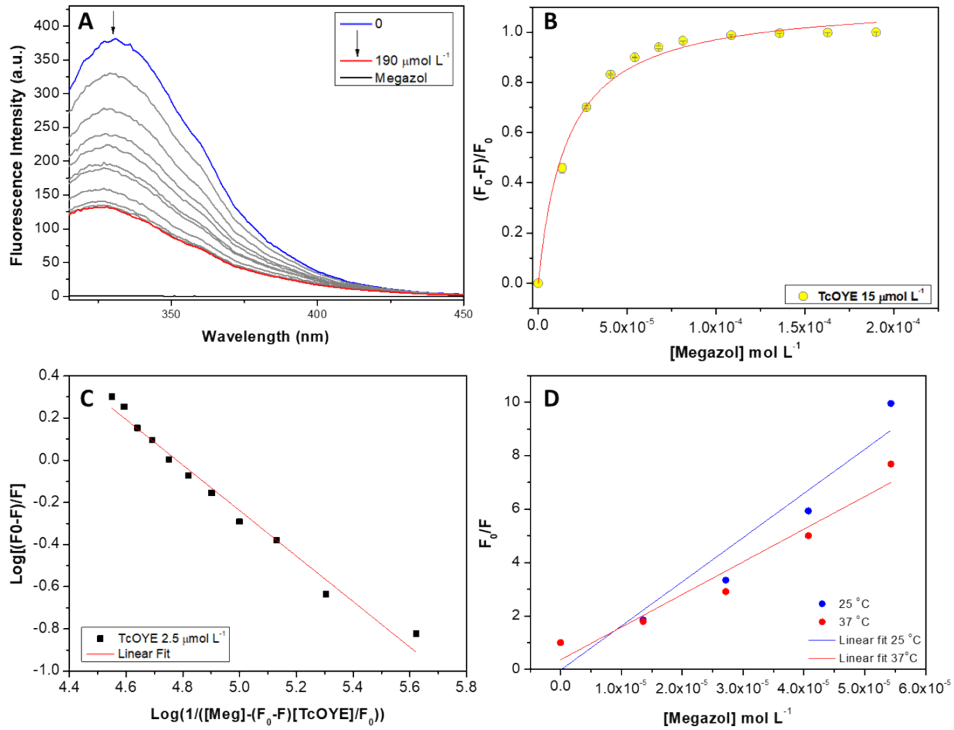

Figure S6.2 - (A) Fluorescence emission spectra (λ_{ex} = 295 nm) of the protein TcOYE at concentration of 15 μmol L^{-1} in the presence of increasing concentrations of megazol. (B) Variation of the intensities of the maximum fluorescence (λ_{max} = 336 nm) and non-linear fit to the Hill equation (Equation 1). (C) Logarithmic relationship for obtaining the number of linking sites according to Equation 2. Stern-Volmer plot at temperatures 25 and 37 °C. The spectra were obtained in Tris-HCl, pH 8.0; 100 mmol L^{-1} of NaCl and 2.5 % of DMSO.

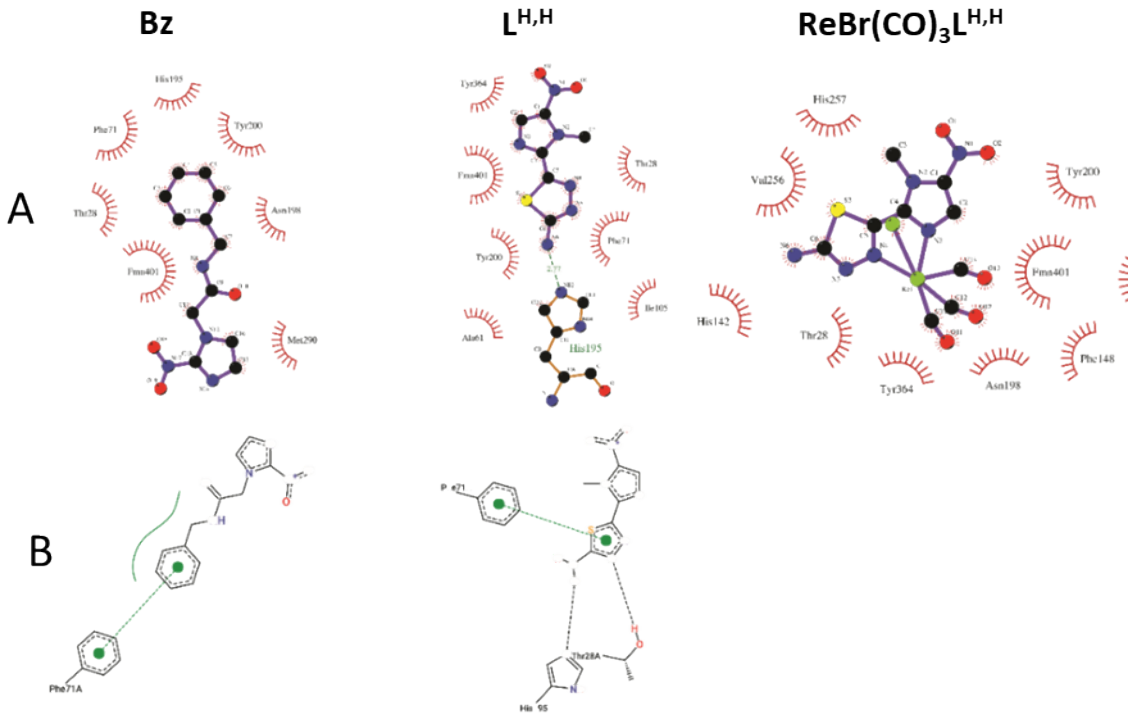

Figure S6.3. Two-dimensional projection of the interaction of compounds with TcOYE/FMN obtained by A) LigPlot software and B) PoseView web server [1,2]. Hydrogen bonds are shown in traced lines, hydrophobic interactions in green and red contours, and π-π interactions on lines traced in green. PoseView did not calculate a two-dimensional projection for the [$ReBr(CO)_3L^{H,H}$] interactions with the enzyme.

PART 7. Radiolabeling data

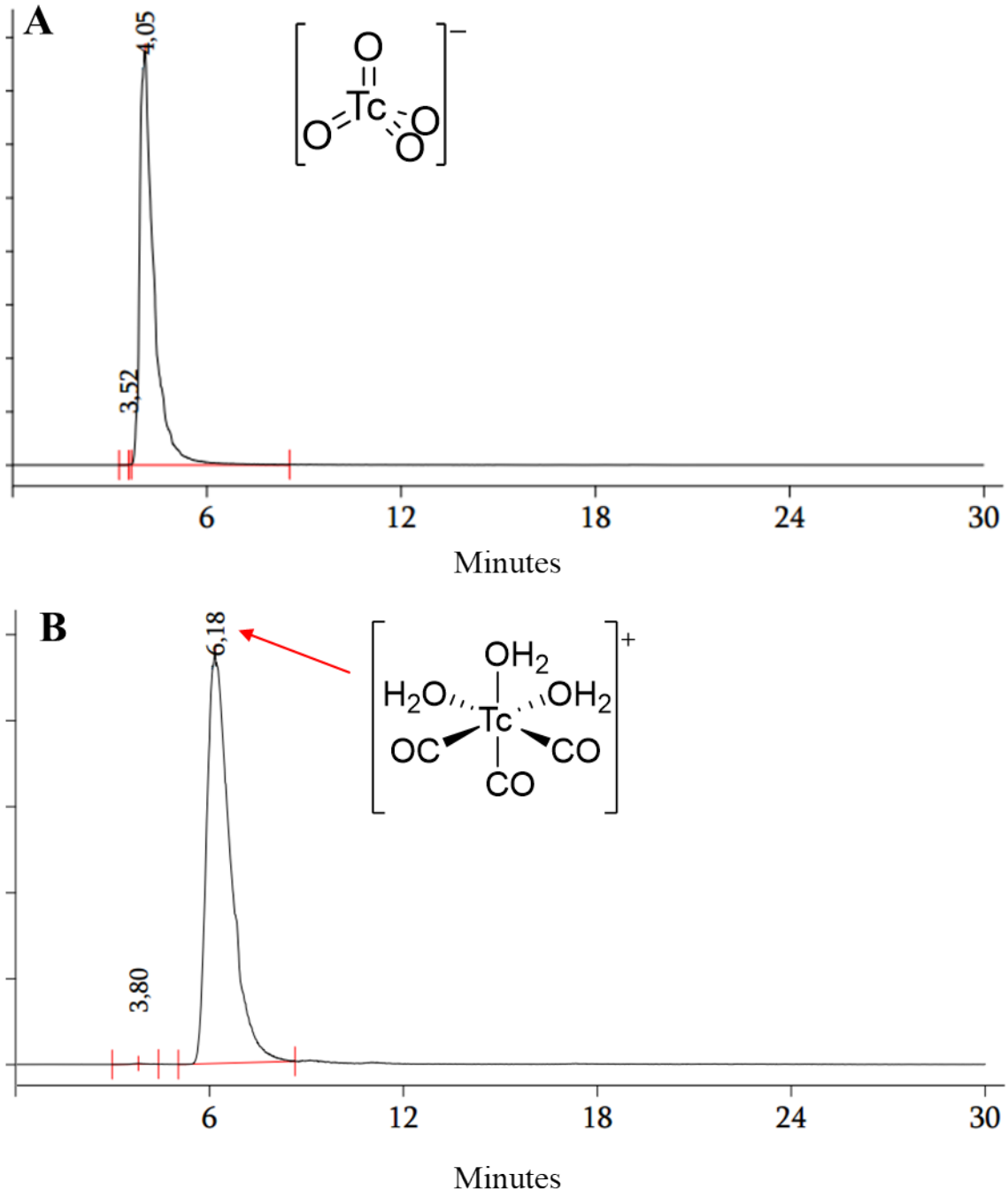

Figure S7.1 – (A) Radio-chromatogram of $[^{99m}TcO_4]^+$ and (B) chromatogram of $[^{99m}Tc(OH_2)_3(CO)_3]^+$. The experiments were performed using a γ detector.

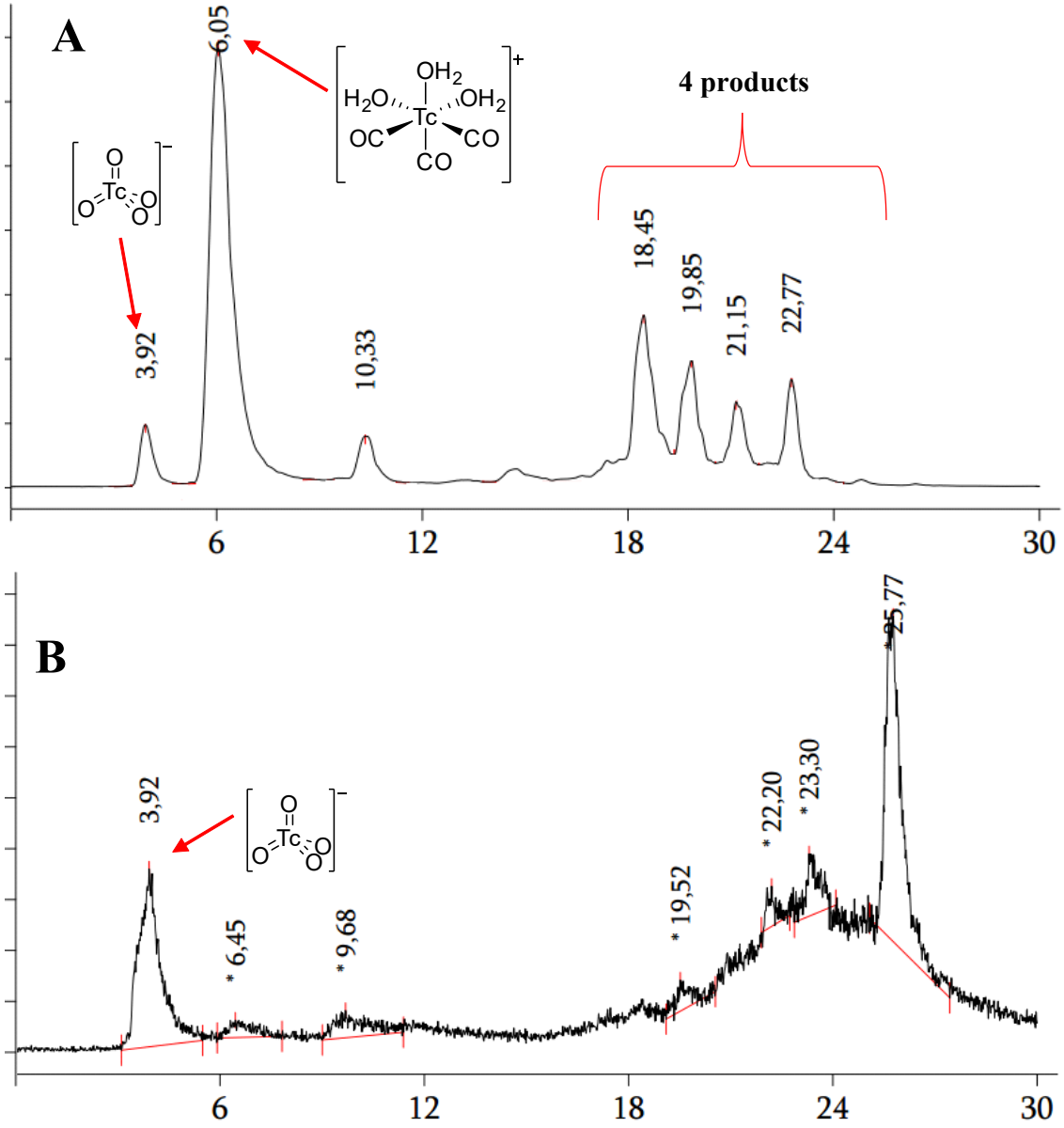

Figure S7.2 – Radio-chromatogram of reaction in basic pH with (A) $L^{H,H}$ and (B) $L^{Me,Me}$. For $[^{99m}Tc(OH_2)_3(CO)_3]^+$ and free ligands 4 products were observed. The experiments were performed using a γ detector.

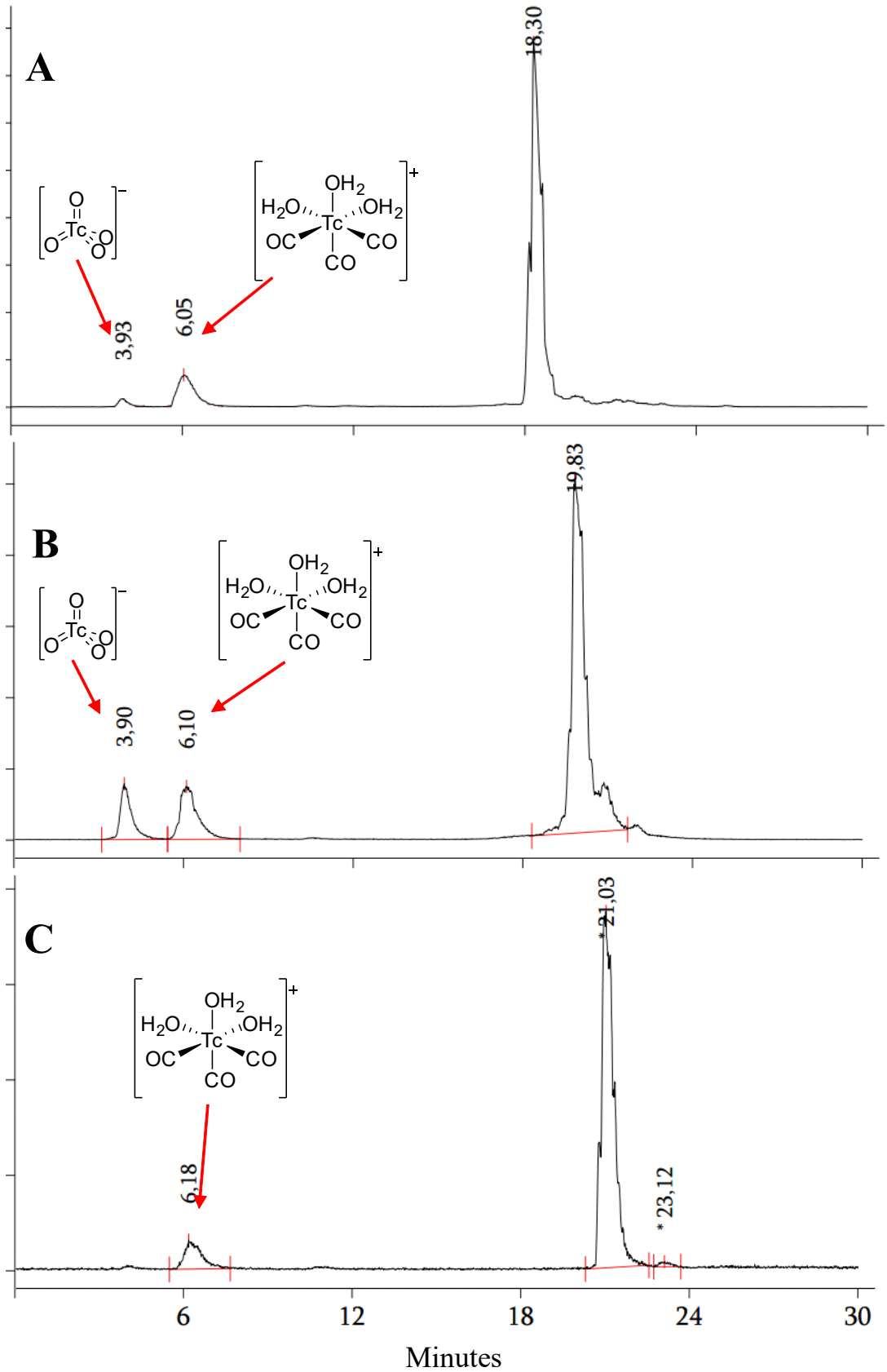

Figure S7.3 – Radio-chromatogram of reaction in acidic pH with (**A**) $\mathbf{L^{H,H}}$ **;** pH 4.0**; yield 48%** (**B**) $\mathbf{L^{H,Me}}$; pH 4.0; yield 45% and (**C**) $\mathbf{L^{Me,Me}}$, pH 2; 14.2% . The reaction resulted in one product. The experiments were performed using a γ detector.

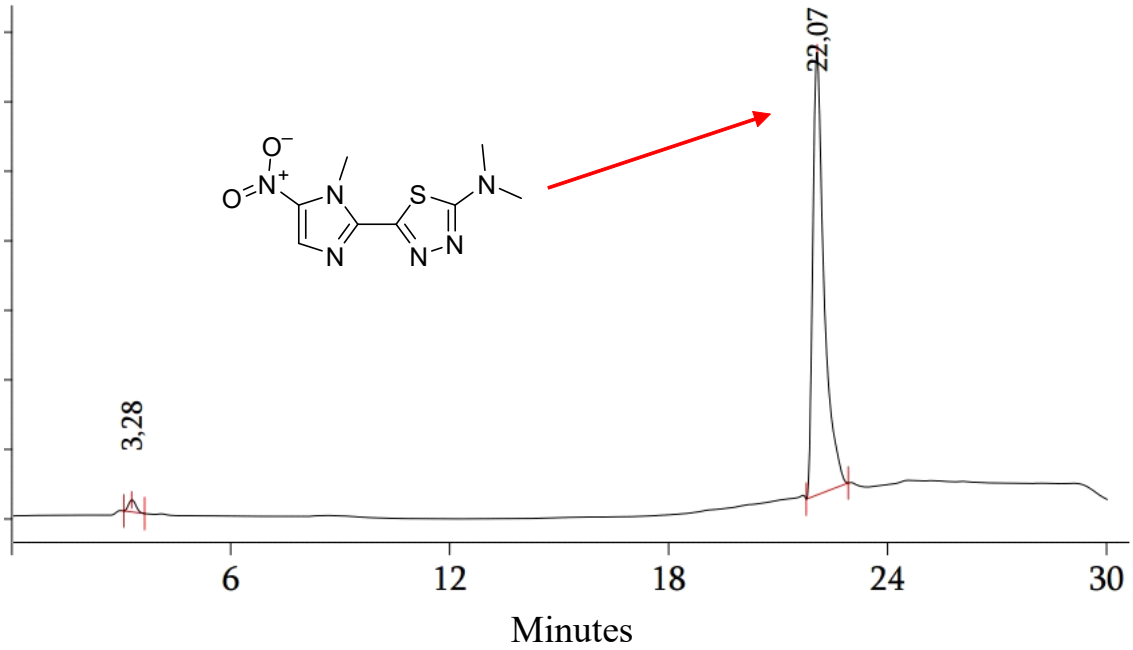

Figure S7.4 –Chromatogram of the compound $L^{Me,Me}$ using UV detector.

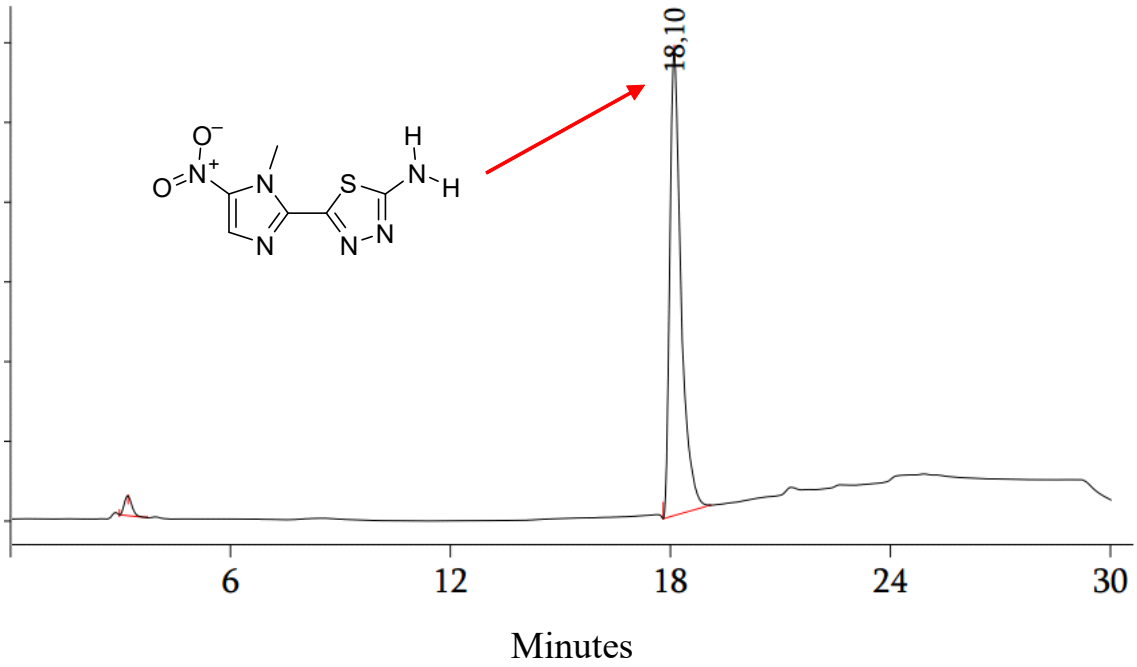

Figure S7.5 –Chromatogram of the compound $L^{H,H}$ using UV detector.

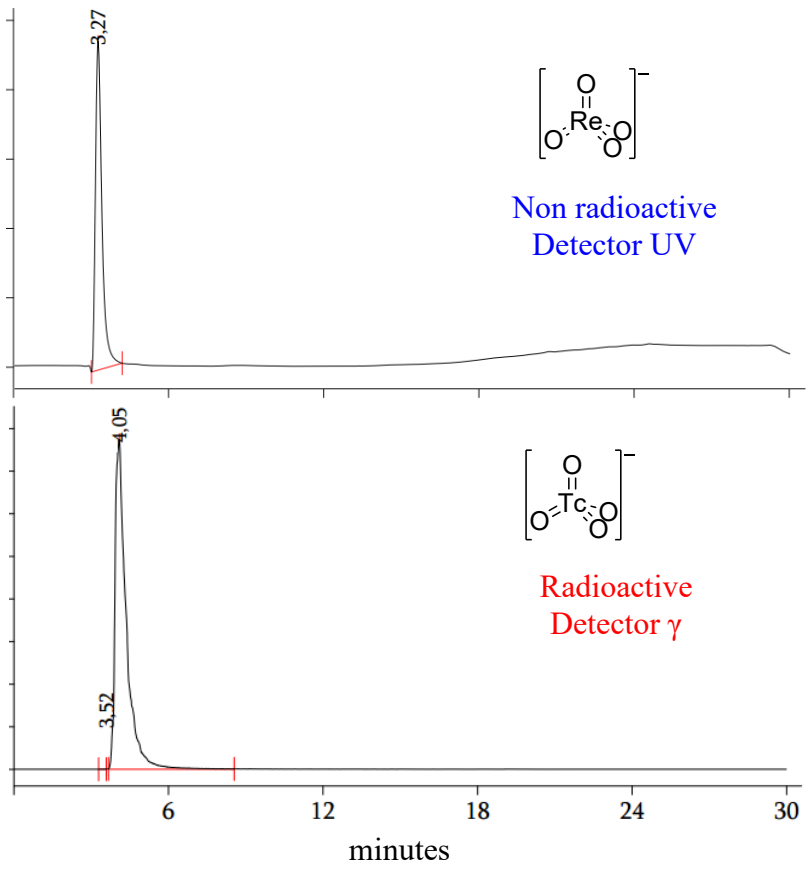

Figure S7.6 – Reference for the analysis of the ^{99m}Tc complexes. Time difference: 0.78 minutes.

Supplementary references

[1] Stierand, K.; Rarey, M. Drawing the PDB: Protein−Ligand Complexes in Two Dimensions. *ACS Med. Chem. Lett.* **2010**, *1*, 540-545. https://doi.org/10.1021/ml100164p

[2] Laskowski, R.A.; Swindells, M.B. LigPlot+: Multiple Ligand–Protein Interaction Diagrams for Drug Discovery. *J. Chem. Inf. Model.* **2011**, *51*, 2778-2786. https://doi.org/10.1021/ci200227u